Article

Cell

A Hardwired HIV Latency Program

Graphical Abstract

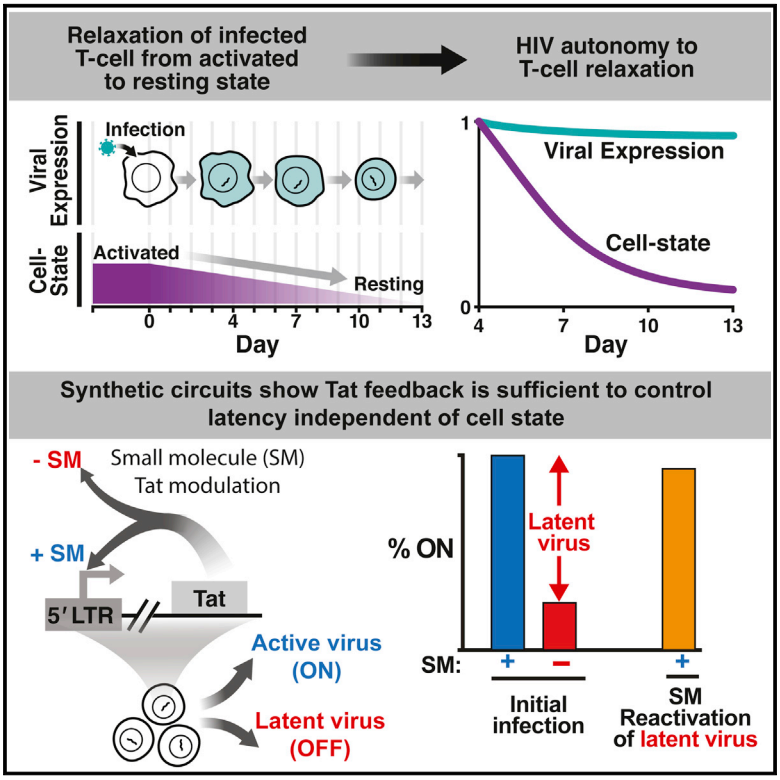

Highlights

- HIV expression persists even when primary cells transition from activated to resting
- Tat positive-feedback circuitry drives this autonomy from cell-state relaxation
- Orthogonal activation of Tat shows that the circuitry suffices for autonomous latency

Authors

Brandon S. Razooky, Anand Pai, ..., Igor M. Rouzine, Leor S. Weinberger

Correspondence

leor.weinberger@gladstone.ucsf.edu

In Brief

Although HIV latency is currently thought to arise when an infected cell transitions from an activated to a resting state that is non-permissive to viral expression, a combination of modeling and synthetic control of HIV Tat positive feedback demonstrates that latency establishment operates autonomously from cell state.

Razooky et al., 2015, Cell *160*, 990–1001
February 26, 2015
http://dx.doi.org/10.1016/j.cell.2015.02.009

CellPress

Cell

Article

A Hardwired HIV Latency Program

Brandon S. Razooky,[1,2,5,6] Anand Pai,[1,3,5] Katherine Aull,[2] Igor M. Rouzine,[1] and Leor S. Weinberger[1,3,4,*]
[1]The Gladstone Institutes (Virology and Immunology), San Francisco
[2]Biophysics Graduate Group
[3]Department of Biochemistry and Biophysics,
[4]QB3
California Institute of Quantitative Biosciences, University of California, San Francisco, 94158
[5]Co-first author
[6]Present address: Laboratory of Immune Cell Epigenetics and Signaling, The Rockefeller University, New York, NY 10065, USA
*Correspondence: leor.weinberger@gladstone.ucsf.edu
http://dx.doi.org/10.1016/j.cell.2015.02.009

SUMMARY

Biological circuits can be controlled by two general schemes: environmental sensing or autonomous programs. For viruses such as HIV, the prevailing hypothesis is that latent infection is controlled by cellular state (i.e., environment), with latency simply an epiphenomenon of infected cells transitioning from an activated to resting state. However, we find that HIV expression persists despite the activated-to-resting cellular transition. Mathematical modeling indicates that HIV's Tat positive-feedback circuitry enables this persistence and strongly controls latency. To overcome the inherent crosstalk between viral circuitry and cellular activation and to directly test this hypothesis, we synthetically decouple viral dependence on cellular environment from viral transcription. These circuits enable control of viral transcription without cellular activation and show that Tat feedback is sufficient to regulate latency independent of cellular activation. Overall, synthetic reconstruction demonstrates that a largely autonomous, viral-encoded program underlies HIV latency—potentially explaining why cell-targeted latency-reversing agents exhibit incomplete penetrance.

INTRODUCTION

Diverse biological systems, both natural and engineered, face the challenge of surviving in variant and unpredictable environmental conditions. One strategy is to sense surrounding conditions and respond with environment-specific developmental programs—there is a 1:1 correspondence between explicit sensor-actuators and the extremely reduced form of this scheme in which sensing and actuation are so tightly coupled that environment entirely actuates the program (Bull and Vogt, 1979). An alternate strategy foregoes environmental sensing and actuation, instead relying on autonomous programs (Knedler, 1947), for example programs that intrinsically generate heterogeneity in phenotypes and allow probabilistic "bet hedging" (Cohen, 1966). For many systems, such as bacteriophage-λ, it is unclear whether environmental sensor-actuator schemes or autonomous programs are employed (Arkin et al., 1998; St-Pierre and Endy, 2008; Zeng et al., 2010). The ensuing debates carry evolutionary significance since sensor-actuator regulation can be driven by crosstalk from coincidental signals and hence tied to unrelated epiphenomena, whereas autonomous circuits are invariably subjected to direct natural selection pressures. In other words, if a phenotype is controlled by sensor-actuator regulation, it can be an "epiphenomenon," but if autonomously regulated, the phenotype is invariably evolutionary hardwired and directly selected for.

For HIV, the debate is clinically relevant; it remains unclear whether the host-cell environment or autonomous viral circuitry controls proviral latency, a long-lived viral dormancy state that is the chief barrier to curative therapy (Richman et al., 2009; Weinberger and Weinberger, 2013). Upon infecting $CD4^+$ T lymphocytes, HIV either actively replicates to rapidly produce progeny virions or can enter a long-lived quiescent state (proviral latency), from which it subsequently reactivates. These latently infected cells form a viral reservoir, forcing patients to remain on lifelong suppressive therapy. The prevailing view (Coffin and Swanstrom, 2013; Siliciano and Greene, 2011) holds that proviral latency results from HIV transcription being controlled by the host-cell activation state (i.e., environment) since relaxation of activated lymphocytes to a resting-memory state is correlated with increased epigenetic silencing of the HIV promoter and increased cytoplasmic sequestration of transcription factors that activate HIV transcription (Pearson et al., 2008; Tyagi et al., 2010). In this model, HIV infects activated T cells, which allow active viral replication, and if these cells "relax" to resting-memory T cells, which generally restrict HIV infection, viral latency ensues (Figure 1, left).

In contrast to the cellular control hypothesis, there is circumstantial evidence for an alternate model wherein latency is controlled by viral gene-regulatory circuitry (Ho et al., 2013; Jeeninga et al., 2008; Weinberger et al., 2005) without strict dependence on cellular state (Figure 1, right). HIV encodes a transcriptional master circuit that is driven by the HIV Tat protein, which amplifies expression from the viral promoter within the HIV long terminal repeat (LTR), establishing positive feedback. Critically, minimal Tat positive-feedback circuits can recapitulate latency, and stochastic fluctuations between a

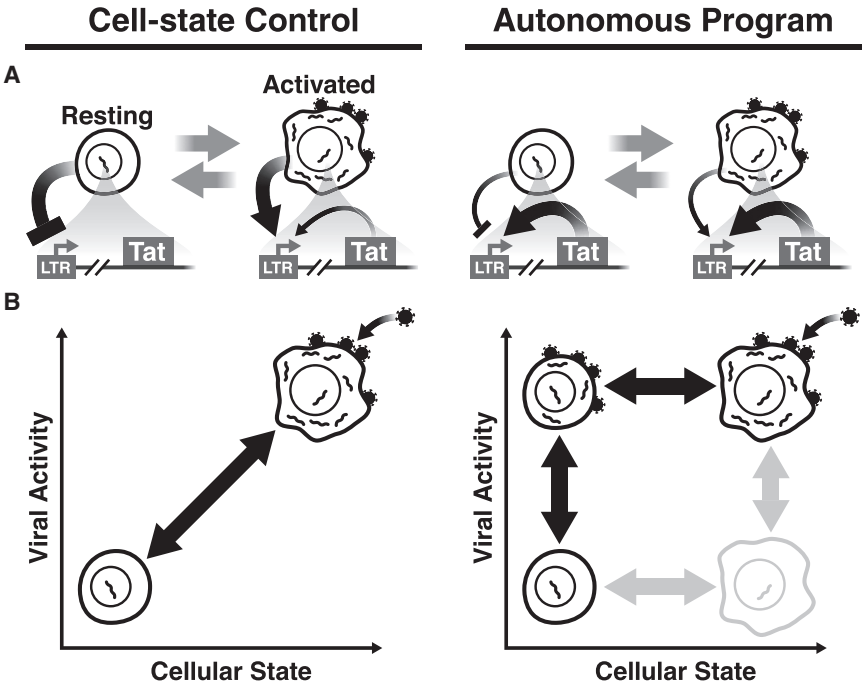

Figure 1. Two Models of HIV Latency Regulation: Cell-State Control versus Autonomous Programming

(A) (Left) The prevailing hypothesis of HIV proviral latency regulation. As $CD4^+$ T cells relax from an activated state (permissive to infection) to a resting-memory state, the host-cell environment silences HIV gene expression, restricting Tat transactivation of the LTR. (Right) The alternate hypothesis that HIV Tat positive feedback is robust to changes of the host-cell environment and operates autonomously despite changes in cell state. The overlapping nature of cellular and viral regulatory circuits confounds testing between these hypotheses (i.e., the LTR actuates Tat feedback but doubles as a sensor of the host-cell environment). (B) If cell state and viral circuitry can be orthogonalized (i.e., decoupled), the influence of cellular state on viral latency can be analyzed via an orthogonal 2D graphical correlation. (Left) If cellular state dominates regulation of viral latency, resting cells would inhibit viral circuitry while active cells would induce viral gene expression, generating a strong correlation between cell state and viral activity. (Right) If an autonomous latency circuit regulates latency, both latent and active viral expression could be generated in either resting cells or activated T cells, producing little correlation between cell state and viral activity.

transcriptionally on and off state in the Tat circuit are sufficient to drive a phenotypic bifurcation between active and latent expression, even in non-resting cells (Weinberger et al., 2005). However, there is also evidence that cellular factors modulate stochastic HIV expression to drive latency (Burnett et al., 2009), confounding the hypothesis that latency is controlled by an autonomous viral circuit.

Here, we test between the cell-state and autonomous-circuit hypotheses for latency establishment. If latency is regulated by host-cell state, viral expression should be tightly correlated with cell state, whereas if the latency circuit is hardwired to function autonomously, then cellular state would be uncorrelated with viral expression and tuning viral circuitry, independent of cell state, would be sufficient to control HIV latency (Figure 1B). Surprisingly, we find that viral expression is robust to cellular-activation state in primary T cells, and mathematical models indicate that this autonomy results from intrinsic properties of the HIV Tat positive-feedback circuit. However, directly testing circuit autonomy to cell state is confounded by overlap between cellular and viral networks—the same transcription factors that alter cellular activation also activate the HIV LTR, triggering Tat positive feedback (Karn, 2011). To circumvent this overlap, we synthetically reconstruct the Tat circuit to decouple viral dependence on the cellular environment from viral transcriptional regulation (i.e., decouple viral sensing and actuation). The refactored circuits chemically modulate viral expression independent of cellular activation levels and show that Tat circuitry is sufficient to overcome cell-driven silencing of HIV transcription during cellular relaxation from active to resting. Overall, the results argue that the Tat circuit is hardwired to establish latency largely autonomous of cellular state.

RESULTS

Donor-Derived Primary T Lymphocytes Maintain Robust HIV Expression during Cellular Relaxation from Activated to Resting

To test the prevailing "epiphenomenon" hypothesis of HIV latency establishment, we αCD3/CD28 pre-activated donor-derived primary human $CD4^+$ T lymphocytes (to achieve a $CD25^+CD69^+$ phenotype), infected them with full-length HIV-1 virus, and then removed activation stimuli, allowing infected cells to relax to a resting ($CD25^-CD69^-$) state (Figure 2A). The virus used (HIV-d2GFP) encodes a short-lived 2-hr half-life GFP (d2GFP) reporter to enable rapid detection of viral transcriptional silencing and is *env* mutated (i.e., single-replication round) to avoid confounding the data with expansion of the infected cell population. Infected cells were sampled periodically over 2 weeks for cellular activation status (as quantified by CD25 and CD69) alongside viral-GFP expression.

Surprisingly, viral expression appears remarkably robust during the cellular transition from activated to resting (Figures 2B and 2C–2H). Despite drastic decline in cellular activation both in CD25 (Figures 2D and 2G) and in CD69 (Figures 2C and 2F), viral activity (quantified by GFP expression of productively infected cells) remained relatively unchanged (Figures 2B, 2E, and 2H). The resilience of viral gene expression despite cellular relaxation is not due to differential relaxation of productively infected cells compared to the overall population, as productively infected cells relax at the same rate as the overall population (Figure S1).

Since human primary cells represent a mixed co-culture (i.e., infected and uninfected subsets of cells), which may obfuscate the interpretation of results (Jordan et al., 2003), we also

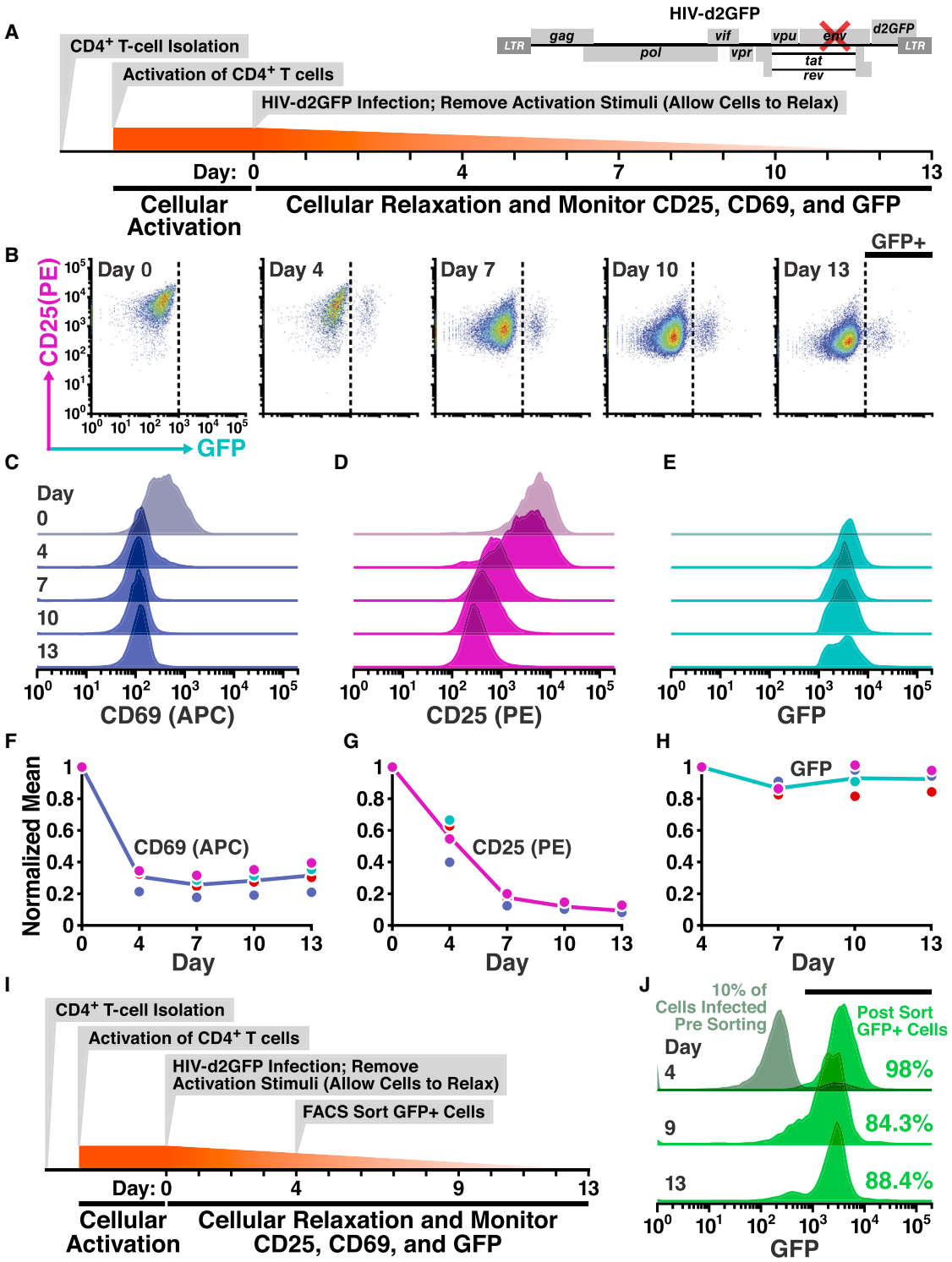

Figure 2. HIV Expression Is Autonomous to Changes in Cellular State: Transitioning of Primary T Lymphocytes from Activated to Resting Does Not Silence HIV Expression

(A) Schematic of activation, infection, and long-term observations of relaxing primary CD4$^+$T cells with full-length HIV-d2GFP. Donor-derived primary cells were activated with αCD3/CD28 beads in the presence of rIL-2 for 3 days, following which beads were removed and the cells were infected. At indicated time points, cells were collected for flow-cytometry-based measurement of CD25/CD69 levels and GFP expression. Data shown (in B–E) are representative of duplicate infections performed with cells from two donors.

(legend continued on next page)

performed a refined version of the experiment by isolating HIV-infected cells through FACS sorting and tracking this purified population of infected lymphocytes as cells relaxed to resting (Figure 2I). As before, even after 2 weeks of culture, ~90% of cells maintain high-level viral expression (Figure 2J) despite cellular relaxation to resting (Figure S1). Collectively, these two experiments show that, despite a 10-fold decline in $CD4^+$ T cell activation levels, the impact on viral gene expression is minimal, suggesting that viral circuitry is largely autonomous to cellular state.

Computational Analysis Predicts that Tat Feedback Circuitry Can Autonomously Generate Active and Latent Infection across a Broad Range of Cellular-Activation States

To investigate how viral transcription remains robust despite cell-state changes, we employ a simplified computational model of HIV transcriptional regulation (Figure 3A) based on previous studies (Weinberger et al., 2008). This model builds off the standard two-state model of transcription (Kepler and Elston, 2001; Paulsson, 2004) and allows the LTR promoter to stochastically toggle between a transcriptionally non-permissive state (LTR_{OFF}) and a transcriptionally permissive state (LTR_{ON}) at rates k_{off} and k_{on}, respectively. In the LTR_{ON} state, Tat protein can transactivate the promoter, enhancing transcriptional elongation at a rate $k_{transact}$. These parameters (k_{off}, k_{on}, and $k_{transact}$) have been quantified by single-cell analysis (Dar et al., 2012; Singh et al., 2010; Weinberger et al., 2008), and measurements at thousands of HIV integration sites across the human genome show k_{on} to be the predominant parameter that alters LTR activity in the regime required for latency (Dar et al., 2012), i.e., the weak expression regime. Potent cell-state activators, such as tumor necrosis factor α (TNFα), which acts through the same pathway as αCD3/CD28 activation, maximally stimulate LTR activity by increasing k_{on} by 1.5- to 2-fold (Dar et al., 2012, 2014; Jordan et al., 2001).

To determine whether relaxation of activated T cells (i.e., decreases in k_{on}) can drive LTR-Tat circuit shutoff and latency, we simulated infection of activated T cells and examined how tuning k_{on} alters the fraction of trajectories in the ON state; i.e., initial conditions were $LTR_{ON} = 1$, and all other molecular species = 0 (see Table S1), thereby allowing efficient Tat turn-on in activated cells with subsequent stochastic circuit shutoff. The simplified model recapitulates previous results showing a phenotypic bifurcation in Tat levels (Weinberger et al., 2005), with a fraction of trajectories remaining ON and a fraction turning OFF (Figure 3B) for any given k_{on} across a broad range of values (Figure 3C). Indeed, for LTR activities within three orders of magnitude (Figure S2), any trajectory can maintain either an ON or OFF state purely by altering the level of Tat without a change in basal LTR activity. Thus, the model predicts that, at a given cellular-activation state (k_{on} value), circuit activity could be toggled ON and OFF simply by supplying Tat alone (e.g., in *trans*) without activating the LTR or changing the cellular-activation state (e.g., via TNFα). Moreover, the ON fraction can also be altered by changing Tat abundance—and hence feedback strength—through Tat half-life modulation (Figure S2).

Next, we directly examined how decreases in k_{on} influenced circuit activity. For all 2-fold decreases in k_{on} (over three orders of magnitude), there is >90% robustness in the percentage of trajectories in the ON state (Figure 3D). 2-fold decreases in LTR activity were examined because removal of cell-state activators (e.g., TNFα), result in 1.5- to 2-fold reductions in LTR activity (Dar et al., 2012; Jordan et al., 2001), but comparable circuit robustness was observed for all 4-fold and even 1-Log reductions in k_{on} (Figure S2). In fact, the simplified nature of the computational model allows derivation of an analytical "closed-form" solution for the fraction of ON trajectories as a function of time for all parameters (see Extended Experimental Procedures), thereby enabling phase-plane analysis of the ON fraction as a function of k_{on} and $k_{transact}$ (Figure S2). This phase-plane sensitivity analysis demonstrates that—throughout the physiological parameter regime of $k_{transact} > k_{on}$ (Dar et al., 2012; Molle et al., 2007)—even if an infected cell lives far longer than the in vivo lifetime of 40 hr (Perelson et al., 1996), k_{on} modulation cannot substantially alter the ON fraction. To be completely sure that these results were not a peculiarity of the specific model used, we also examined an alternate positive-feedback model topology (Weinberger et al., 2005)—which encodes substantially more molecular detail but is experimentally validated—and we observed similar circuit robustness to decreases in k_{on} (Figure S2). Analytical solution shows that this robustness results from the strong positive feedback ($k_{transact} > k_{on}$), since changes in k_{on} produce small corrections. Notably, despite the circuit's robustness to cellular relaxation (k_{on} decreases), high values of k_{on} do generate less-frequent latency in both the simplified model (Figure 3C) and the complex models (Weinberger et al., 2005). In fact, the analytical solution quantifies how increases in k_{on} (e.g., via NFκB stimulation) reactivate the circuit from a latent state (Equation 12, Extended Experimental Procedures).

Overall, the results demonstrate robustness of LTR-Tat circuit activity to cellular relaxation (i.e., reductions in k_{on}), consistent with primary cell observations (Figure 2), but, critically, also

(B) Flow cytometry time course of CD25 and GFP levels taken on indicated days post infection. Dotted line indicates gating for productively infected cells (GFP^+).
(C–E) Histograms of cellular activation levels CD25 (C) and CD69 (D) of the entire population alongside GFP expression from productively infected cells (cells in GFP^+ gate in B) over the course of 13 days post infection (17 days post cellular activation).
(F-H) Cellular activation levels and GFP levels for all replicates over the experimental time course. Each dot indicates the time point from an independent infection and represents the geometric mean of the distribution as seen in C–E. Solid line connects the mean of the replicates. CD25 and CD69 normalized to day 0 (maximal); GFP normalized to day 4 when viral activity is first observed.
(I) Schematic of FACS-based isolation of productively infected cells. 4 days post infection, GFP^+ cells were isolated and cultured (repeated for two donors).
(J) Histograms of isolated GFP^+ cells over time. Numbers indicate the proportion of cells that fall within the gate for positive GFP expression (marked by horizontal black bar). Day 4: Gray histogram shows the infected population prior to FACS-based separation. Viral titer was calibrated to achieve 10% infection (fraction of gray histogram that is GFP^+ at day 4). Histogram in green (for days 4, 9, and 13) shows the GFP expression in the isolated productively infected cells (post sort). All data shown above are from donor 1.
See Figure S1 for results from donor 2 and CD25 expression decline during the experiment.

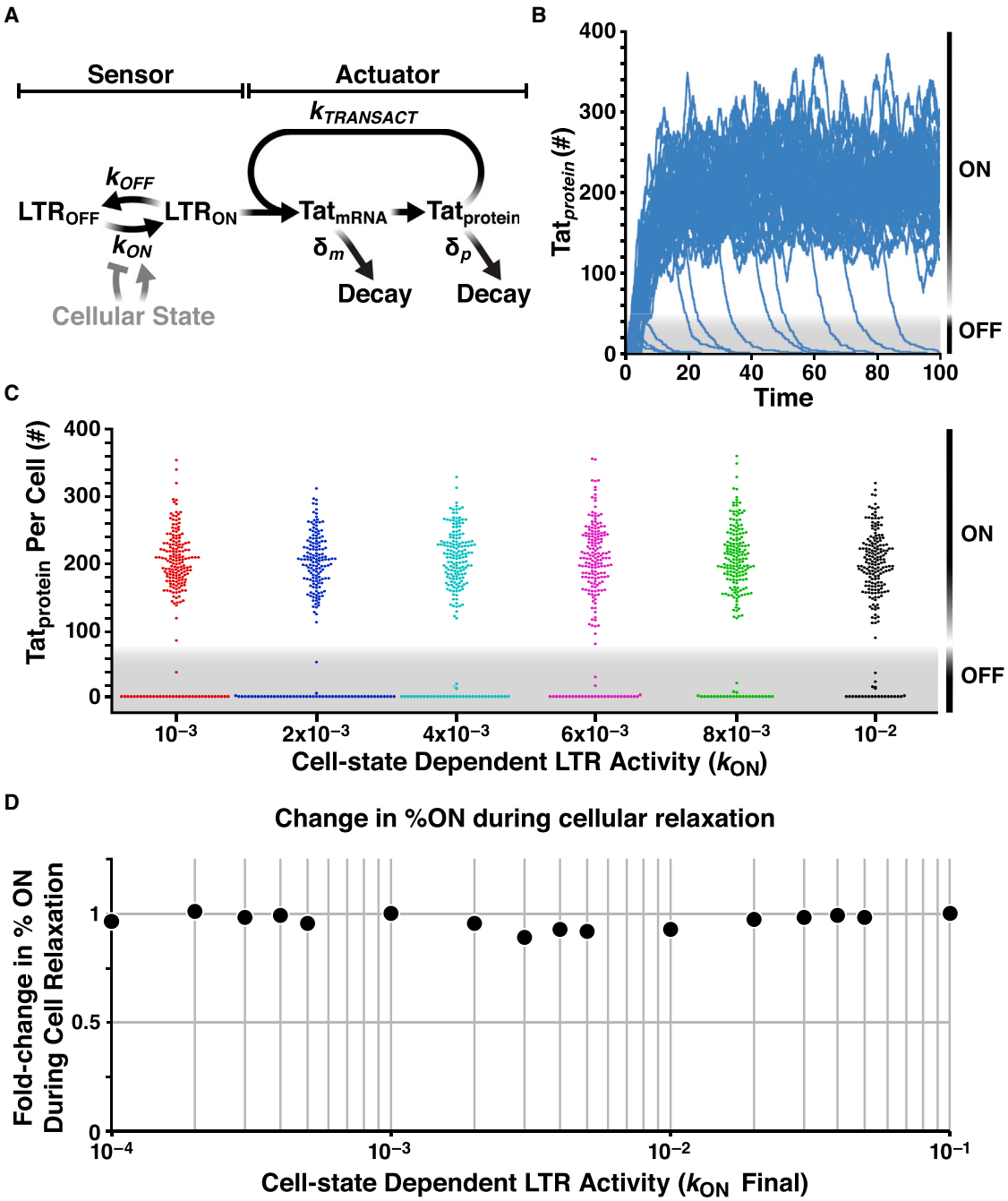

Figure 3. Computational Analysis Predicts that Tat Positive-Feedback Circuitry Underlays HIV Autonomy to Cell State

(A) Schematic of a simplified model of the Tat-feedback circuit. The LTR promoter can toggle between a state where transcriptional elongation is stalled (LTR_{OFF}) and a state where elongation proceeds (LTR_{ON}) at rates k_{off} and k_{on}, respectively, (Dar et al., 2012; Singh et al., 2010, 2012) and Tat protein transactivates the promoter by enhancing transcriptional elongation at a rate $k_{transact}$ (Razooky and Weinberger, 2011). Tat protein and mRNA decay at rates δ_m and δ_p, respectively.

(B) Stochastic Monte-Carlo simulations ("Gillespie" algorithm) of Tat protein levels (in arbitrary number of molecules) in individual cells over time (from reaction scheme in A). Each trajectory represents an individual cell; 100 single-cell trajectories shown (initial conditions for all species equal zero at time t = 0, except $LTR_{ON} = 1$); see Extended Experimental Procedures for reaction rates.

(C) Bee-Swarm plots of circuit activity (Tat levels at t = 200) over a range of k_{on} values. Each data point represents a single-cell trajectory, (200 trajectories shown per k_{on} value). The width of the collection of cells (dots) having zero level of Tat (bottom of each k_{on} value simulated) shows that high values of k_{on} do generate less frequent latency (smaller number of dots). Compare, for example, the spread of red dots ($k_{on} = 10^{-3}$) and black dots ($k_{on} = 10^{-2}$) at 0.

(legend continued on next page)

show sensitivity of latency to changes in Tat abundance or changes in Tat half-life. Below, we experimentally test these computational predictions: (1) that LTR-Tat circuit activity between latent and active can be toggled by Tat levels alone (i.e., independent of cellular-activation state), (2) that Tat is more effective at activation from latency than cell-state modifiers, and (3) that cellular relaxation to resting does not silence Tat positive-feedback circuitry.

A Minimal Synthetic Circuit Shows that Viral Reactivation from Latency Can Be Toggled Independent of Cellular Activation

To test whether HIV gene-regulatory circuitry can control proviral latency without changes in cellular-activation state, we developed synthetic circuits in which viral expression could be toggled independent of cell state. The synthetic circuits are based upon a minimal model of the HIV latency circuit and encode a transcriptional positive-feedback loop in which HIV Tat amplifies expression from the HIV LTR promoter (Jordan et al., 2001; Weinberger et al., 2005). The minimal LTR-Tat circuit is sufficient to recapitulate latent gene expression; stimulation with cell-state modifiers reactivates proviral expression from a non-expressive "OFF" state to a high-level "ON" state.

The minimalist synthetic toggle circuit encodes Tat fused to a controllable proteolysis tag, FKBP (Banaszynski et al., 2006), under the control of the HIV LTR (Figure 4A). FKBP degradation is reversibly inhibited by a small molecule, Shield-1, allowing Tat half-life to be rapidly tuned. The Tat-FKBP fusion was also tagged with a photo-switchable fluorescent protein, Dendra-2 (Gurskaya et al., 2006), which allows for light-based pulse-chase experiments (Zhang et al., 2007) to measure Tat half-life destabilization in single cells (Figure S3). In this minimal LTR-Tat-Dendra-FKBP viral vector, Tat half-life is reduced to 2.5 hr in the absence of Shield-1 (a ~3.3-fold reduction from its native half-life) but returns to its native 8 hr half-life (Weinberger and Shenk, 2007) in the presence of 1 μM Shield-1.

Simulations predict that changes in Tat half-life should be sufficient to toggle HIV positive feedback between ON and OFF at a majority of viral integration sites (Figure S2). As predicted, altering the Tat half-life by addition or removal of Shield-1 was sufficient to toggle between latent and active expression across an array of integration sites (Figure 4B). The observed reactivation is not due to pleiotropic effects of Shield-1 since Tat-Dendra fusion proteins lacking FKBP are insensitive to Shield-1 (Figure S3). Moreover, the increased expression levels cannot simply be due to an increase in the half-life of the reporter (Dendra-2), as the expression increases are substantially greater than the 3.3-fold increase in half-life caused by Shield-1 (Figure S3). To be completely sure that reporter half-life changes were not accounting for the increased expression, we also decoupled the fluorescent reporter half-life from the Tat half-life by creating a polycistronic system in which the reporter protein and Tat are transcriptionally fused, but not translationally fused (Figure S4). The polycistronic system corroborates the finding that Tat positive feedback is sufficient to control viral switching from an inexpressive OFF to expressive ON state (Figure S4). Thus, in both the translational and transcriptional fusions, Shield-1 toggles the circuit between ON and OFF. These data indicate that tuning Tat positive feedback is sufficient to toggle HIV gene expression between a quiescent state and an actively expressing state and that viral expression can be activated without activating cell state.

Tat Induction Alone Is More Efficient Than Cell-State Activation for Reactivating Latent Clones

One caveat of using tunable proteolysis systems to toggle the Tat circuit is that a minimal level of Tat protein must be present in the off state—i.e., modulating protein half-life when protein concentration is zero has no effect. Thus, the Tat-FKBP approach is unable to test whether Tat can reactivate latent cells that are fully silenced. To circumvent this obstacle and test whether Tat induction is sufficient to reactivate completely silenced LTRs, we developed a set of open-loop circuits, based on the Tet-On system (Gossen and Bujard, 1992), that induce Tat expression de novo. These systems allow tight induction of Tat expression upon Doxycycline (Dox) addition. To examine the effects of Tat induction on HIV gene expression, these circuits were incorporated into cells that encoded an HIV LTR promoter driving the mCherry fluorescent reporter (Figure 4C), and a library containing 33 distinct LTR clonal integration sites was examined.

The Tet-On circuits show that Tat by itself is sufficient to toggle cells between OFF and ON and to control the mean levels of LTR expression despite the large clonal variation (Figure 4D). Importantly, a number of clones (clones 1–3) exhibit no detectable LTR expression in the absence of Tat induction—the conventional threshold for latency. But, inducing Tat expression is sufficient to fully reactivate these clones without the need for any cell-state activation signals.

Next, to test the effects of cell-state activation, Tet-inducible isoclonal populations were exposed to an array of standard cell-state modifiers. These agents are potent activators of T lymphocytes (Pazin et al., 1996) and also of the LTR (Jordan et al., 2001; Karn, 2011). For example, TNFα strongly activates T cell state by stimulating nuclear localization of the nuclear factor of activated T cells (NFAT) and by stimulating recruitment of the p50-RelA heterodimer to promoters containing NF-κB-binding sites (Karin and Lin, 2002). If cell-state activation were the dominant factor controlling latency, then cell-state modulators should strongly reactivate latent mCherry expression in the Tet-inducible system. Strikingly, cell-state activation alone only slightly increases LTR expression and the percentage of cells in the ON state, across the library of 33 distinct integration sites (Figure 4E). In contrast, induction of Tat (by Dox) drastically increases the percentage of cells in the ON state to near 100% (Figure 4E). This dramatic difference between direct Tat induction versus cell-state modifiers demonstrates that $k_{transact} > k_{on}$ for the HIV circuitry and indicates that Tat-mediated transactivation is far

(D) Fold change in percentage of trajectories in ON state for 2-fold reductions in k_{on}. Circuit activity (%ON) is largely robust to reductions in LTR activity (i.e., k_{on}) over three orders of magnitude. Phase-plane analysis (i.e., sensitivity analysis) from a closed-form analytical solution shows that this behavior is robust across the physiological parameter regime ($k_{transact} > k_{on}$).
See also Figure S2 and Table S1.

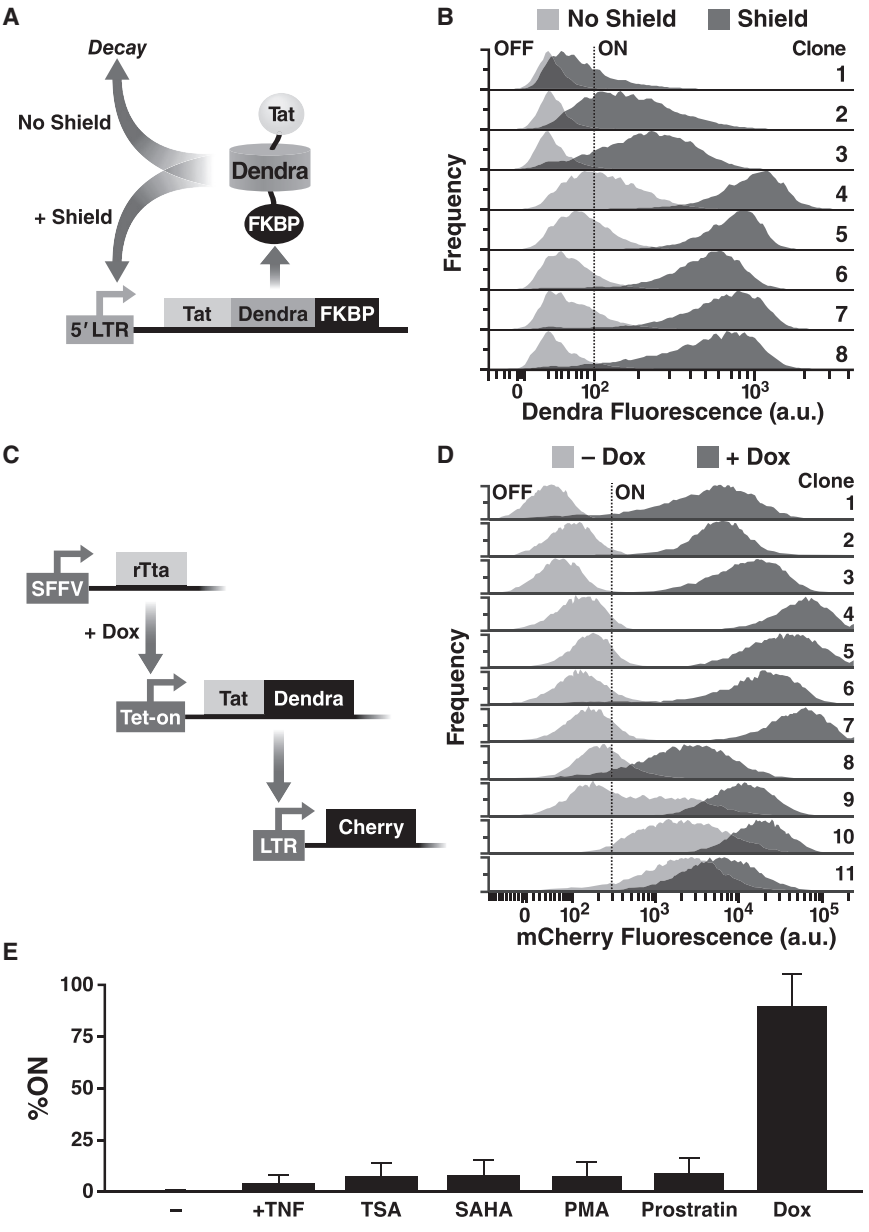

Figure 4. Synthetic Tuning of Tat Circuit Activity Is Sufficient to Control Latent HIV Expression in the Absence of Cellular Activation

(A) Schematic of the minimal LTR-Tat-Dendra-FKBP lentiviral circuit. In the absence of Shield-1, the Tat-Dendra-FKBP fusion protein is rapidly degraded, diminishing positive feedback. When Shield-1 is added, FKBP-mediated proteolysis is blocked, allowing Tat levels to increase and enabling strong Tat positive feedback.

(B) Flow cytometry histograms of eight isoclonal populations of Jurkat cells infected with LTR-Tat-Dendra-FKBP in the absence of Shield-1 (light gray histograms) or the presence of 1 μM Shield-1 (dark gray histograms). Gating of the Dendra-positive region (right of black-dashed line) was set relative to naive, un-transduced Jurkat cells. See also Figures S3 and S4.

(C) Schematic of the synthetic system (left) and flow cytometry data of the LTR expression in cells transduced with the synthetic circuit (right). The synthetic circuit is composed of an rTta activator constitutively expressed from an SFFV promoter. In the presence of Dox, rTta protein activates the Tet-On promoter to drive expression of the Tat-Dendra fusion protein. Tat transactivates expression from the HIV-1 LTR promoter, and LTR activity is measured by mCherry expression.

(D) LTR mCherry expression is shown for 11 representative isoclonal populations in the absence of Dox (light gray histograms) or after Dox addition (dark gray histograms).

(E) Flow cytometry analysis of a library containing 33 distinct LTR clonal integration sites subjected to Dox and a panel of standard cell-state modifiers: TNFα, phorbol myristate acetate (PMA), PMA-ionomycin, suberanilohydroxamic acid (SAHA/vorinostat), trichostatin A (TSA), or prostratin.

Error bars show SD.

stronger an effect than the switching of the LTR to an ON state through cell-state modifications. Collectively, these data (Figure 4E) indicate that activating cell-state alone is not sufficient to control HIV transcription. These results in no way exclude a role for cellular state in HIV reactivation in vivo. Rather, the sufficiency of Tat-mediated viral reactivation without cell-state modification emphasizes the autonomy of the HIV Tat circuit.

Refactoring of Full-Length Replicating HIV Indicates that Latency Establishment and Reactivation Depend on Viral-Circuit Activity and Are Largely Independent of Cellular Activation

We next tested whether viral circuitry could control latency in full-length replicating virus. First, we developed a decoupled system in which Tat expression is controlled by the cells (via Tet-On) completely independently of the virus. The engineered cells, termed "inducible Tat cells," contain a stable integrated Tet-inducible Tat-Dendra cassette and provide in *trans* complementation of Tat for a reengineered Tat-deleted full-length virus, the ΔTat-Cherry virus. The ΔTat-Cherry virus was constructed from a full-length HIV molecular clone containing a Tat deletion (Huang et al., 1994) and encodes an mCherry fluorescent reporter within *nef* (Figure 5A). In these inducible Tat cells, viral gene expression can be toggled on even if initial Tat levels are zero and virus replicates only in the presence of Dox and, as with conventional strains, virus is inhibited by HIV protease inhibitors (Figure S5). Inducing Tat expression in these cells during infection with ΔTat-Cherry virus shows a ~400% increase in active infection compared to non-induced ΔTat Cherry-infected cells (Figure 5B), indicating that absence of Dox drives the virus to enter latency in agreement with findings that Tat protein can inhibit establishment of latency (Donahue et al.,

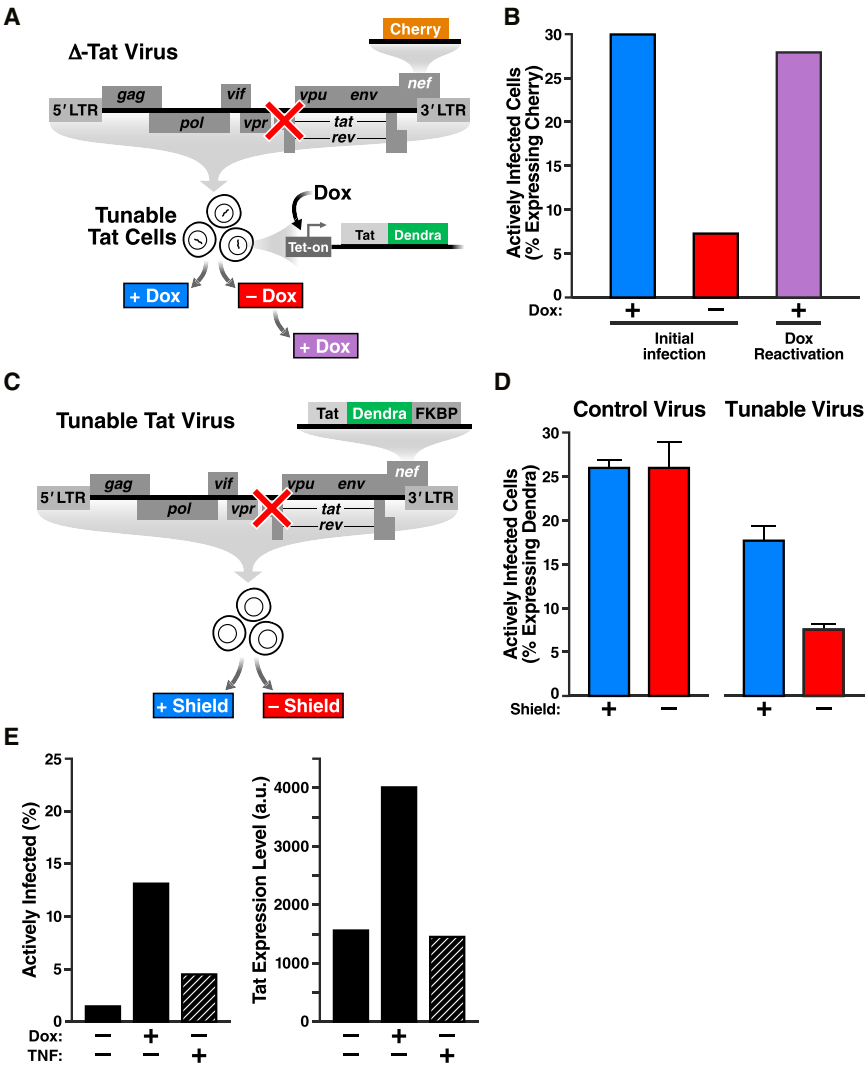

Figure 5. Tat Feedback Circuitry Is Sufficient to Control Active-versus-Latent Infection in Full-Length Viruses

(A) Schematic of experiment: A Jurkat cell line in which Tat-Dendra is expressed only in the presence of Dox, "inducible Tat cells," was infected with full-length ΔTat-Cherry virus in the presence (+) or absence (–) of Dox to score for latency and to score reactivation. Dox– infections were subsequently induced by Dox.

(B) Percent of cells actively infected (actively expressing mCherry) 2 days post infection. 30% of cells were actively infected in the presence of Dox (blue), while only 7% of cells were actively infected in the absence of Dox (red). Upon subsequent Dox incubation of the Dox– infection, 28% of cells reactivated to active infection (purple), indicating that virtually all latent cells can be reactivated with Tat induction.

(C) Experiment schematic: CEM T cells were infected with either full-length Tat-FKBP virus or control virus in the presence or absence of Shield-1.

(D) Percent of cells actively infected (actively expressing Dendra) 2 days post infection. For the control virus infection, 25.8% ± 1.0% of cells exhibit active infection in the presence of 1 μM Shield-1 (blue), while 26.0% ± 2.7% exhibit active infection in the absence of Shield-1 (red). For the Tat-FKBP virus infection, 17.5% ± 1.7% of cells exhibit active infection in the presence of 1 μM Shield-1 (blue), while 7.5% ± 1.0% of cells exhibit active infection in the absence of Shield-1 (red). Infections were performed in triplicate. Error bars = 1 SD. Control virus infection and Tat-FKBP virus infection are independent experiments (infection titers of the two are different).

(E) Comparison of viral circuit versus cell-state activation by quantifying the percentage of delta-Tat virus infections that enter the active state. In the absence of TNFα or Dox, 2% of cells generate active HIV replication. Dox addition increases active infections to ~13%, while TNFα generates 4% actively infected cells. The same can be seen by plotting Tat expression level (Dendra). Again, TNFα by itself leaves expression level unchanged over that in absence of treatment. Addition of Dox leads to >2-fold increase in expression.

Also see Figure S5 for the experiment repeated with Dox and a panel of cell-state modifiers.

2012). Strikingly, subsequent induction of Tat expression by Dox fully reactivates latent virus to levels observed in the initial infection with Dox (Figure 5B). Further, Dox was far more effective in reactivating latent virus than any of the standard cell-state modifiers: TNFα, PMA, PMA-ionomycin, SAHA/vorinostat, TSA, or prostratin (Figure S5). Hence, latent provirus can be reactivated by Tat induction alone, without altering cellular-activation state, demonstrating that Tat is sufficient to control latent reactivation in full-length HIV.

Next, to check whether Tat induction in *cis* (i.e., within the positive-feedback loop) could also control latency in full-length virus, we reengineered the ΔTat-Cherry virus to encode either the Tat-Dendra-FKBP cassette, referred to as "Tat-FKBP virus" (Figure 5C), or a control Tat-Dendra cassette, referred to as "Tat-Dendra control virus," or simply "control virus" (Figure S5). As previously established in these *nef*-reporter viruses, actively replicating infections express reporter, while latent infections are quantified by absence of reporter expression (Jordan et al., 2003; Pearson et al., 2008). In control HIV infections, Shield-1 has no measureable effect on active-versus-latent infection (Figure 5D). In striking contrast, in Tat-FKBP virus infections, modulating Tat positive-feedback strength with Shield-1 alters the percentage of actively infected cells by 141%, i.e., >2-fold (Figure 5D). The reduction in actively infected cells is not due to reduced input virus since equivalent titers of virus (i.e., MOIs) were used in the presence and absence of Shield-1 and the lack of measureable difference in infection in control HIV infections indicates that Shield-1 is not inducing abortive infections and that hypothetical pleiotropic effects of Shield-1 cannot explain the difference in active-versus-latent infection. Overall, these results show that modulating viral feedback strength is sufficient to control the establishment of active-versus-latent infection in full-length replicating virus.

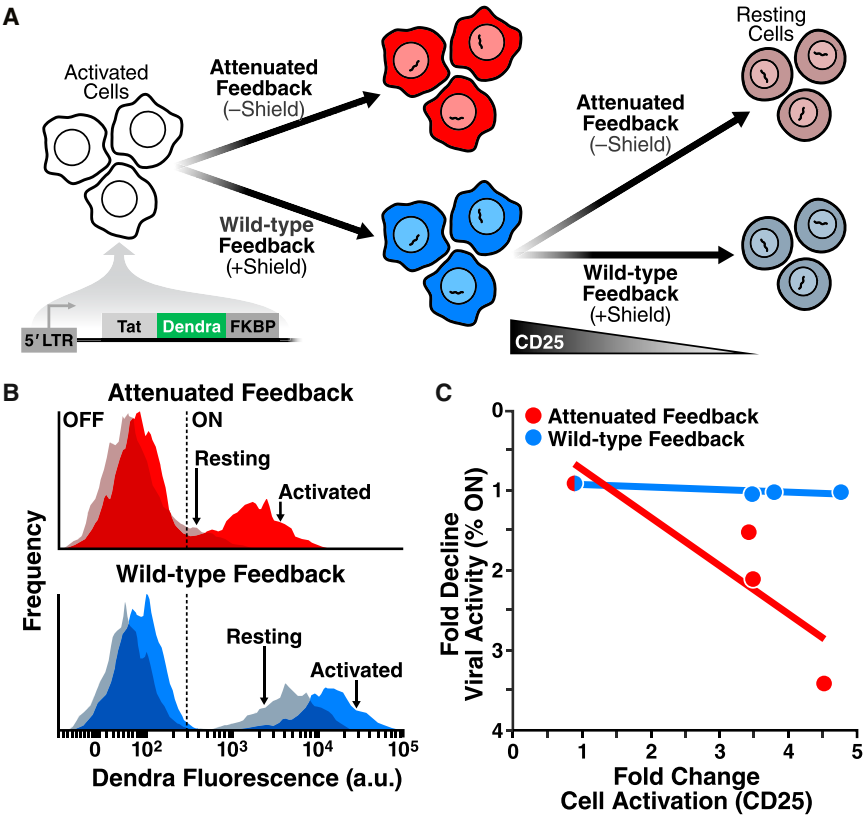

Figure 6. Tat Feedback Circuitry Is Sufficient to Autonomously Regulate Viral Expression during the Activated-to-Resting Transition in Primary T Cells

(A) Experiment schematic: Donor-derived primary CD4$^+$ T lymphocytes were activated and infected with LTR-Tat-Dendra-FKBP in either the presence of Shield-1 (blue, wild-type feedback) or without Shield (red, attenuated feedback), and cells were allowed to relax back to resting (as measured by CD25 surface expression) in the presence/absence of Shield-1 (i.e., under wild-type/attenuated feedback).

(B) Flow cytometry analysis of viral expression (Dendra fluorescence) in primary CD4$^+$ T lymphocytes during transition from activated to resting in absence of Shield-1 (attenuated feedback; top) or presence of Shield-1 (wild-type feedback; bottom); activated are lymphocytes shown as opaque histograms, and resting lymphocytes are shown as translucent histograms.

(C) Plot of the fold change in the number of active infections for varying cellular state (fold change cell activation as measured by CD25 surface expression; see also Figure S6). If feedback strength is wild-type (blue data points; blue trend line), the fold change in viral activity is uncorrelated with changing cell state. In the presence of attenuated feedback, the percentage of active infections is dependent on cell state. Each data point is normalized against the percent of active infections in the lowest cell-state activation data point.

Tat Induction Is >300% More Effective Than Cellular Activation for Reactivating Full-Length Latent HIV

To directly compare the effects of tuning viral circuitry to altering cellular-activation state, inducible Tet-Tat-Dendra cells were infected with ΔTat virus in the presence of Dox or TNFα (Figure 5E). Modifying cellular activity with TNFα, in the absence of Tat induction, leads to a 1.5-fold change in the percentage of active infections (from 2% to 4% active infection), whereas Tat induction drastically increases, by >300%, the proportion of infections that are active (Figure 5E). Similar results were seen in reactivating latent cells post infection (Figure S5): inducible Tet-Tat-Dendra cells were infected with ΔTat virus and 3 days post infection were treated with either Dox or standard cell-state modulators (as well as combination of the two). Tat induction through Dox was significantly more effective at reactivation than the cell-state modifiers. Thus, as seen with the minimal-synthetic circuits (Figure 4), perturbing viral circuitry provides substantially more potent reactivation of latency than targeting cell state alone.

Tat Circuitry Is Sufficient to Autonomously Regulate Viral Expression during the Activated-to-Resting Transition in Human Primary T Lymphocytes

As a final test, we directly examined the model prediction that Tat circuitry alone is sufficient to explain the resilience of HIV transcription to cellular silencing during cellular relaxation from activated to resting (Figure 3D). Activated primary CD4$^+$ T cells were transduced with LTR-Tat-Dendra-FKBP virus and allowed to relax from an active to a resting-memory state while Tat positive-feedback strength was either maintained or attenuated by removing Shield-1 (Figure 6A).

When Tat positive feedback is attenuated (by absence of Shield-1) as lymphocytes relax from activated to memory, significant silencing of HIV gene expression occurs (Figure 6B, red histograms). However, when Tat positive-feedback strength is maintained at wild-type levels (via Shield-1 addition), only a slight shift in HIV gene expression occurs as lymphocytes transition from active to memory (Figure 6B, blue histograms). Quantifying the relaxation of cellular activation alongside viral latency reveals a remarkable relationship: if Tat feedback is attenuated, the cellular-activation state tightly controls entry to latency by significantly reducing the percentage of cells in active infection (Figure 6C, red); however, when Tat feedback is active (the case in Figure 2), the cellular activation state has no bearing on entrance into latency as the percentage of cells in active infection remains constant (Figure 6C, blue)—i.e., the intact feedback circuit allows viral gene expression to act completely independent of cellular-activation state. Thus, active Tat feedback appears to buffer HIV from global transcriptional silencing as primary lymphocytes transition from active to resting memory.

DISCUSSION

Beginning with observations that HIV gene expression is largely autonomous to cellular relaxation (Figure 2), computationally guided synthetic reconstruction revealed Tat positive feedback as the core mechanism underlying viral autonomy

(Figures 3–5). Strikingly, Tat feedback alone is sufficient to overcome cell-driven silencing of HIV transcription during cellular relaxation from active to resting in primary T cells (Figure 6). These findings are consistent with patient-cell latent-reactivation experiments showing that direct addition of Tat activates viral expression and reverses latency in resting $CD4^+$ T cells without requiring cellular activation (Lassen et al., 2006; Lin et al., 2003). Thus, in patient cells, Tat-mediated positive feedback also appears to regulate latency independent of cell state.

The data herein cannot discount one variant of the cell-state hypothesis which proposes that latency is established when HIV infects relaxing cells which are at an activation level just above a first threshold required for HIV infection and integration but below a second threshold required to sustain active Tat expression and viral replication. However, there are difficulties with this hypothesis. While the presence of two thresholds is plausible, the second (Tat activation) threshold being higher than the first (infection) threshold is not consistent with existing data. For example, although global activation of primary $CD4^+$ T cells is required for efficient infection, HIV can be reactivated from latency in primary cells without globally activating the cells (Xing et al., 2012). Similarly, the reactivation of HIV in resting T cells using Tat protein (Lassen et al., 2006; Lin et al., 2003) indicates that extremely low levels of cellular activation (i.e., in resting/quiescent cells) are still amenable to robust viral expression. Thus, since resting cells are at an activation level non-permissive to infection (Pan et al., 2013) but are sufficiently activated for Tat to function, the putative Tat-activation threshold is *lower* than the infection threshold and the two-threshold scenario appears unlikely.

If cellular relaxation does not lead to the establishment of HIV latency, how is HIV latency established? Previous studies demonstrated the intrinsic ability of the Tat positive-feedback circuit to rapidly and stochastically establish latency (Weinberger et al., 2005), consistent with recent primate studies showing that latency is rapidly established within the first 3 days of infection (Whitney et al., 2014) and with cell-culture models showing latency establishment immediately upon infection (Calvanese et al., 2013; Dahabieh et al., 2013). Given that resting $CD4^+$ T lymphocytes are highly resistant to direct HIV infection (Pan et al., 2013), the rapid establishment of latency is difficult to reconcile with the cell-state epiphenomenon theory; productively infected cells live <2 days in vivo (Perelson et al., 1997), while the process of T cell transitioning from active to memory is a slow and low-probability process (Youngblood et al., 2013) occurring during and after vigorous expansion of effector lymphocytes that only begins weeks after infection (Kuroda et al., 1999). The alternate model examined here (Figure 3), wherein intrinsic (stochastic) viral circuitry autonomously regulates HIV latency, also provides a mechanistic basis for recent observations in patient cells (Ho et al., 2013), showing that: (1) a significant fraction of latent proviruses are not induced even if cells are reactivated from a resting-memory state, and (2) a second identical cellular stimulation (of already activated cells) induces additional latent proviruses to reactivate. These results indicate that viral reactivation is probabilistic. While particularly puzzling for the cellular-control hypothesis, probabilistic reactivation is consistent with HIV latency being regulated by an autonomous viral-encoded circuit influenced by stochastic gene-expression fluctuations, which provides rationale for targeting viral gene-expression circuitry to reactivate latent HIV (Dar et al., 2014).

To be completely clear, the viral-encoded latency model does not exclude a role for cellular state in regulating HIV proviral latency. In fact, the Tat-feedback model predicts that latency establishment is sharply reduced at higher cellular activation levels (Figure 3C) and that cellular activation probabilistically reactivates latent virus (Equation 12 in Extended Experimental Procedures). Experimentally, cellular activation clearly rescues attenuated feedback (Figure 6B). Similarly, the ability of Tat expression to reactivate latent virus independent of cellular activation (Figures 4 and 5) does not imply that in vivo latent reactivation occurs absent cellular activation. Rather, the results herein demonstrate—contrary to prevailing dogma—that there is also an underlying viral program that autonomously regulates proviral latency.

A viral-encoded latency program naturally raises questions on the evolutionary origin and function of HIV latency. While sensor-actuator circuitry would have been consistent with either the epiphenomenon hypothesis or evolutionary hardwiring, an autonomous regulatory circuit is invariably hardwired and must be selectively maintained—especially in a rapidly evolving virus under strong selection. So, how would latency be beneficial in the natural history of lentiviral infection? In a companion paper (Rouzine et al., 2015 [this issue of *Cell*]), we propose that latency may provide a fitness advantage by acting as a viral "bet-hedging" strategy to enhance net viral transmission probability. An associated aspect is the decision-making architecture behind latency: Tat positive feedback maintains strong expression levels robust to cellular perturbations, while large stochastic fluctuations exhibited by the LTR promoter enable the system to probabilistically switch (Dar et al., 2012). Notably, this architecture has been theoretically proposed to be an unreliable environmental sensor in fluctuating environments (Brandman et al., 2005), suggesting that HIV's circuit architecture is precisely the *opposite* configuration that would be required for a reliable environmental sensor—a reliable sensor would respond faithfully to environmental changes—and similar stochastic positive-feedback circuitry has been proposed for autonomous decision making in other biological systems (Jilkine et al., 2011). Overall, viral evolution appears to have selected for circuitry that both maintains remarkable autonomy from environmental cues and simultaneously drives probabilistic on-off decision making.

EXPERIMENTAL PROCEDURES

Primary-Cell Isolation and Cell-Culture Conditions

Primary $CD4^+$ T cells were isolated from peripheral blood obtained from Stanford Blood Bank (Palo Alto, CA) using RosetteSep Human $CD4^+$ T Cell Enrichment Cocktail from STEMCELL Technologies and Ficoll as described (Terry et al., 2009). Once isolated, cells were either cultured as described (Terry et al., 2009) or frozen in 10% DMSO, 90% culture media at a density of 10^7 per ml. For infections, primary $CD4^+$ T cells were pre-activated for 2–3 days with αCD3/CD28 beads (Dynabeads, Life Technologies) as per manufacturer's instructions. Cell activation was measured

by flow cytometry with anti-CD25-PE-conjugated antibody and anti-CD69-APC-conjugated antibody from BD Biosciences. Primary $CD4^+$ T lymphocytes, Jurkat T Lymphocytes, and CEMs were all cultured in RPMI 1640 (supplemented with L-glutamine, 10% fetal bovine serum, and 1% penicillin-streptomycin) in a humidified environment at 37°C and 5% CO_2. Jurkats and CEM were maintained by passage between 2×10^5 and 2×10^6 cells/ml. Primary cell media was supplemented with 20 U/ml r-IL2 (Peprotech, 200-02).

Computational Modeling

A simplified two-state model of Tat positive feedback was constructed from experimental data of LTR toggling (Dar et al., 2014; Dar et al., 2012; Singh et al., 2010; Singh et al., 2012) and simulated using the Gillespie algorithm (Gillespie, 1977) to test how altering LTR basal transcription rate or Tat protein stability would affect the activity of the circuit. The chemical reaction scheme and parameters used are described in Table S1. The outputs from simulations are the different molecular species in arbitrary numbers. Stochastic simulations were run in Mathematica using the xSSA package (http://www.wolfram.com/mathematica/ and http://www.xlr8r.info/SSA/). Initial conditions for all species were set to 0, except for LTR_{ON}, which was set to 1, and simulations were run to time = 200 (arbitrary time units); 500 simulation runs were conducted for each parameter set. See Extended Experimental Procedures for further details and explanation of simulations for the more complex model (Figure S2).

Recombinant Virus Production and Infections

Lentivirus was packaged in 293T cells and isolated as described (Dull et al., 1998; Weinberger et al., 2005). HIV-d2GFP (Jordan et al., 2003) was packaged with dual-tropic *env*-encoding plasmid pSVIII-92HT593.1 (NIH AIDS Reagents Program). Before infecting primary cells, activation beads were removed and cells were mixed with appropriate amount of virus (to get <10% infection) in 100 μl media and spinoculated at 32°C for 2 hr at 1,000 × *g*.

To generate the isoclonal populations with engineered viral circuits, lentivirus was added to Jurkat T Lymphocytes at a low MOI to ensure a single integrated copy of proviral DNA in infected cells. Cells were stimulated with tumor necrosis factor α (TNFα) and Shield-1 for 18 hr before sorting for Dendra-expressing cells. Isoclonal and polyclonal populations were created as described (Weinberger et al., 2005). Sorting and analysis of cells infected was performed on a FACSAria II. The same procedure was followed to create the LTR-Tat-Dendra and LTR-mCherry-IRES-Tat-FKBP cell lines. Inducible Tat cells were generated by transducing Jurkat cells with Tet-Tat-Dendra and SFFV-rTta lentivirus at high MOI. The cells were incubated in Dox for 24 hr and then FACS sorted for $Dendra^+$ cells to create a polyclonal population. To create the Tet-Tat-Dendra + LTR-mCherry cells, the polyclonal population was infected with LTR-mCherry lentivirus at a low MOI. Before sorting for $mCherry^+$ and $Dendra^+$ cells, Dox was added at 500 ng/ml for 24 hr, and single cells were FACS sorted and expanded to isolate isoclonal populations. The same procedure was followed for the Tet-Tat-Dendra-FKBP + LTR-mCherry populations; however, 24 hr before the sort, 1 uM Shield-1 and 500 ng/ml Dox was added to the culture. All inducible Tat or control HIV infection experiments were performed by incubating 5×10^5 CEM cells in the same titer of inducible Tat or the same titer of control HIV in the presence or absence of Shield-1 and taking a flow cytometry time point after 48 hr. Δ-Tat mCherry infections were carried out using 10^5–10^6 inducible Tat (Jurkat) cells in the presence or absence of 500 ng/ml doxycycline.

Flow Cytometry and Analysis

Flow cytometry data were collected on a BD FACSCalibur DxP8, BD LSR II, or HTFC Intellicyt for stably transduced lines and primary cells and on a BD FACSAria II for replication-competent virus assays and sorting. All flow cytometry experiments on replication-competent virus were performed in BSL3 conditions (safety information available upon request). Flow cytometry data were analyzed in FlowJo and using customized MATLAB code.

SUPPLEMENTAL INFORMATION

Supplemental Information includes Extended Experimental Procedures, six figures, and one table and can be found with this article online at http://dx.doi.org/10.1016/j.cell.2015.02.009.

AUTHOR CONTRIBUTIONS

B.S.R., A.P., and L.S.W. designed research and wrote the paper. B.S.R., A.P., and K.A. executed the experiments and analyzed the data. I.M.R., B.S.R., and L.S.W. performed mathematical analysis.

ACKNOWLEDGMENTS

We are grateful to M. Thompson, O. Weiner, J. Toettcher, J. Miranda, A. Weinberger, M. Ott, E. Verdin, A. Frankel, M. Simpson, and G. Süel for comments, helpful discussions, and providing reagents. B.S.R. was supported by an NSF graduate research fellowship (GRFP, grant 1144247). This work was supported by NIH award R01-AI109593 and, in part, by the Center for Synthetic and Systems Biology at UCSF (P50GM081879), the NIH Delaney CARE Collaboratory of AIDS Researchers for a Cure (U19AI096113), and UCSF-GIVI CFAR (P30AI027763 and S10RR028962-01). L.S.W. acknowledges support from NIH Director's New Innovator Award Program (DP2-OD006677), the Alfred P. Sloan Foundation, and the Pew Scholar's in the Biomedical Sciences.

Received: September 2, 2014
Revised: December 9, 2014
Accepted: February 5, 2015
Published: February 26, 2015

REFERENCES

Arkin, A., Ross, J., and McAdams, H.H. (1998). Stochastic kinetic analysis of developmental pathway bifurcation in phage lambda-infected Escherichia coli cells. Genetics *149*, 1633–1648.

Banaszynski, L.A., Chen, L.C., Maynard-Smith, L.A., Ooi, A.G., and Wandless, T.J. (2006). A rapid, reversible, and tunable method to regulate protein function in living cells using synthetic small molecules. Cell *126*, 995–1004.

Brandman, O., Ferrell, J.E., Jr., Li, R., and Meyer, T. (2005). Interlinked fast and slow positive feedback loops drive reliable cell decisions. Science *310*, 496–498.

Bull, J.J., and Vogt, R.C. (1979). Temperature-dependent sex determination in turtles. Science *206*, 1186–1188.

Burnett, J.C., Miller-Jensen, K., Shah, P.S., Arkin, A.P., and Schaffer, D.V. (2009). Control of stochastic gene expression by host factors at the HIV promoter. PLoS Pathog. *5*, e1000260.

Calvanese, V., Chavez, L., Laurent, T., Ding, S., and Verdin, E. (2013). Dual-color HIV reporters trace a population of latently infected cells and enable their purification. Virology *446*, 283–292.

Coffin, J., and Swanstrom, R. (2013). HIV pathogenesis: dynamics and genetics of viral populations and infected cells. Cold Spring Harb. Perspect. Med. *3*, a012526.

Cohen, D. (1966). Optimizing reproduction in a randomly varying environment. J. Theor. Biol. *12*, 119–129.

Dahabieh, M.S., Ooms, M., Simon, V., and Sadowski, I. (2013). A doubly fluorescent HIV-1 reporter shows that the majority of integrated HIV-1 is latent shortly after infection. J. Virol. *87*, 4716–4727.

Dar, R.D., Razooky, B.S., Singh, A., Trimeloni, T.V., McCollum, J.M., Cox, C.D., Simpson, M.L., and Weinberger, L.S. (2012). Transcriptional burst frequency and burst size are equally modulated across the human genome. Proc. Natl. Acad. Sci. USA *109*, 17454–17459.

Dar, R.D., Hosmane, N.N., Arkin, M.R., Siliciano, R.F., and Weinberger, L.S. (2014). Screening for noise in gene expression identifies drug synergies. Science *344*, 1392–1396.

Donahue, D.A., Kuhl, B.D., Sloan, R.D., and Wainberg, M.A. (2012). The viral protein Tat can inhibit the establishment of HIV-1 latency. J. Virol. *86*, 3253–3263.

Dull, T., Zufferey, R., Kelly, M., Mandel, R.J., Nguyen, M., Trono, D., and Naldini, L. (1998). A third-generation lentivirus vector with a conditional packaging system. J. Virol. *72*, 8463–8471.

Gillespie, D.T. (1977). Exact Stochastic Simulation of Coupled Chemical-Reactions. J. Phys. Chem. *81*, 2340–2361.

Gossen, M., and Bujard, H. (1992). Tight control of gene expression in mammalian cells by tetracycline-responsive promoters. Proc. Natl. Acad. Sci. USA *89*, 5547–5551.

Gurskaya, N.G., Verkhusha, V.V., Shcheglov, A.S., Staroverov, D.B., Chepurnykh, T.V., Fradkov, A.F., Lukyanov, S., and Lukyanov, K.A. (2006). Engineering of a monomeric green-to-red photoactivatable fluorescent protein induced by blue light. Nat. Biotechnol. *24*, 461–465.

Ho, Y.C., Shan, L., Hosmane, N.N., Wang, J., Laskey, S.B., Rosenbloom, D.I., Lai, J., Blankson, J.N., Siliciano, J.D., and Siliciano, R.F. (2013). Replication-competent noninduced proviruses in the latent reservoir increase barrier to HIV-1 cure. Cell *155*, 540–551.

Huang, L.M., Joshi, A., Willey, R., Orenstein, J., and Jeang, K.T. (1994). Human immunodeficiency viruses regulated by alternative trans-activators: genetic evidence for a novel non-transcriptional function of Tat in virion infectivity. EMBO J. *13*, 2886–2896.

Jeeninga, R.E., Westerhout, E.M., van Gerven, M.L., and Berkhout, B. (2008). HIV-1 latency in actively dividing human T cell lines. Retrovirology *5*, 37.

Jilkine, A., Angenent, S.B., Wu, L.F., and Altschuler, S.J. (2011). A density-dependent switch drives stochastic clustering and polarization of signaling molecules. PLoS Comput. Biol. *7*, e1002271.

Jordan, A., Defechereux, P., and Verdin, E. (2001). The site of HIV-1 integration in the human genome determines basal transcriptional activity and response to Tat transactivation. EMBO J. *20*, 1726–1738.

Jordan, A., Bisgrove, D., and Verdin, E. (2003). HIV reproducibly establishes a latent infection after acute infection of T cells in vitro. EMBO J. *22*, 1868–1877.

Karin, M., and Lin, A. (2002). NF-kappaB at the crossroads of life and death. Nat. Immunol. *3*, 221–227.

Karn, J. (2011). The molecular biology of HIV latency: breaking and restoring the Tat-dependent transcriptional circuit. Curr. Opin. HIV AIDS *6*, 4–11.

Kepler, T.B., and Elston, T.C. (2001). Stochasticity in transcriptional regulation: origins, consequences, and mathematical representations. Biophys. J. *81*, 3116–3136.

Knedler, J.W. (1947). Masterworks of Science—Digests of 13 Great Classics (Garden City, NY: Doubleday & Company).

Kuroda, M.J., Schmitz, J.E., Charini, W.A., Nickerson, C.E., Lifton, M.A., Lord, C.I., Forman, M.A., and Letvin, N.L. (1999). Emergence of CTL coincides with clearance of virus during primary simian immunodeficiency virus infection in rhesus monkeys. J. Immunol. *162*, 5127–5133.

Lassen, K.G., Ramyar, K.X., Bailey, J.R., Zhou, Y., and Siliciano, R.F. (2006). Nuclear retention of multiply spliced HIV-1 RNA in resting CD4+ T cells. PLoS Pathog. *2*, e68.

Lin, X., Irwin, D., Kanazawa, S., Huang, L., Romeo, J., Yen, T.S., and Peterlin, B.M. (2003). Transcriptional profiles of latent human immunodeficiency virus in infected individuals: effects of Tat on the host and reservoir. J. Virol. *77*, 8227–8236.

Molle, D., Maiuri, P., Boireau, S., Bertrand, E., Knezevich, A., Marcello, A., and Basyuk, E. (2007). A real-time view of the TAR:Tat:P-TEFb complex at HIV-1 transcription sites. Retrovirology *4*, 36.

Pan, X., Baldauf, H.M., Keppler, O.T., and Fackler, O.T. (2013). Restrictions to HIV-1 replication in resting CD4+ T lymphocytes. Cell Res. *23*, 876–885.

Paulsson, J. (2004). Summing up the noise in gene networks. Nature *427*, 415–418.

Pazin, M.J., Sheridan, P.L., Cannon, K., Cao, Z., Keck, J.G., Kadonaga, J.T., and Jones, K.A. (1996). NF-kappa B-mediated chromatin reconfiguration and transcriptional activation of the HIV-1 enhancer in vitro. Genes Dev. *10*, 37–49.

Pearson, R., Kim, Y.K., Hokello, J., Lassen, K., Friedman, J., Tyagi, M., and Karn, J. (2008). Epigenetic silencing of human immunodeficiency virus (HIV) transcription by formation of restrictive chromatin structures at the viral long terminal repeat drives the progressive entry of HIV into latency. J. Virol. *82*, 12291–12303.

Perelson, A.S., Neumann, A.U., Markowitz, M., Leonard, J.M., and Ho, D.D. (1996). HIV-1 dynamics in vivo: virion clearance rate, infected cell life-span, and viral generation time. Science *271*, 1582–1586.

Perelson, A.S., Essunger, P., Cao, Y., Vesanen, M., Hurley, A., Saksela, K., Markowitz, M., and Ho, D.D. (1997). Decay characteristics of HIV-1-infected compartments during combination therapy. Nature *387*, 188–191.

Razooky, B.S., and Weinberger, L.S. (2011). Mapping the architecture of the HIV-1 Tat circuit: A decision-making circuit that lacks bistability and exploits stochastic noise. Methods *53*, 68–77.

Richman, D.D., Margolis, D.M., Delaney, M., Greene, W.C., Hazuda, D., and Pomerantz, R.J. (2009). The challenge of finding a cure for HIV infection. Science *323*, 1304–1307.

Rouzine, I., Weinberger, A.D., and Weinberger, L.S. (2015). An evolutionary role for HIV latency in enhancing viral transmission. Cell *160*, this issue, 1002–1012.

Siliciano, R.F., and Greene, W.C. (2011). HIV latency. Cold Spring Harb. Perspect. Med. *1*, a007096.

Singh, A., Razooky, B., Cox, C.D., Simpson, M.L., and Weinberger, L.S. (2010). Transcriptional bursting from the HIV-1 promoter is a significant source of stochastic noise in HIV-1 gene expression. Biophys. J. *98*, L32–L34.

Singh, A., Razooky, B.S., Dar, R.D., and Weinberger, L.S. (2012). Dynamics of protein noise can distinguish between alternate sources of gene-expression variability. Mol. Syst. Biol. *8*, 607.

St-Pierre, F., and Endy, D. (2008). Determination of cell fate selection during phage lambda infection. Proc. Natl. Acad. Sci. USA *105*, 20705–20710.

Terry, V.H., Johnston, I.C., and Spina, C.A. (2009). CD44 microbeads accelerate HIV-1 infection in T cells. Virology *388*, 294–304.

Tyagi, M., Pearson, R.J., and Karn, J. (2010). Establishment of HIV latency in primary CD4+ cells is due to epigenetic transcriptional silencing and P-TEFb restriction. J. Virol. *84*, 6425–6437.

Weinberger, L.S., and Shenk, T. (2007). An HIV feedback resistor: auto-regulatory circuit deactivator and noise buffer. PLoS Biol. *5*, e9.

Weinberger, A.D., and Weinberger, L.S. (2013). Stochastic fate selection in HIV-infected patients. Cell *155*, 497–499.

Weinberger, L.S., Burnett, J.C., Toettcher, J.E., Arkin, A.P., and Schaffer, D.V. (2005). Stochastic gene expression in a lentiviral positive-feedback loop: HIV-1 Tat fluctuations drive phenotypic diversity. Cell *122*, 169–182.

Weinberger, L.S., Dar, R.D., and Simpson, M.L. (2008). Transient-mediated fate determination in a transcriptional circuit of HIV. Nat. Genet. *40*, 466–470.

Whitney, J.B., Hill, A.L., Sanisetty, S., Penaloza-MacMaster, P., Liu, J., Shetty, M., Parenteau, L., Cabral, C., Shields, J., Blackmore, S., et al. (2014). Rapid seeding of the viral reservoir prior to SIV viraemia in rhesus monkeys. Nature *512*, 74–77.

Xing, S., Bhat, S., Shroff, N.S., Zhang, H., Lopez, J.A., Margolick, J.B., Liu, J.O., and Siliciano, R.F. (2012). Novel structurally related compounds reactivate latent HIV-1 in a bcl-2-transduced primary CD4+ T cell model without inducing global T cell activation. J. Antimicrob. Chemother. *67*, 398–403.

Youngblood, B., Hale, J.S., and Ahmed, R. (2013). T-cell memory differentiation: insights from transcriptional signatures and epigenetics. Immunology *139*, 277–284.

Zeng, L., Skinner, S.O., Zong, C., Sippy, J., Feiss, M., and Golding, I. (2010). Decision making at a subcellular level determines the outcome of bacteriophage infection. Cell *141*, 682–691.

Zhang, L., Gurskaya, N.G., Merzlyak, E.M., Staroverov, D.B., Mudrik, N.N., Samarkina, O.N., Vinokurov, L.M., Lukyanov, S., and Lukyanov, K.A. (2007). Method for real-time monitoring of protein degradation at the single cell level. Biotechniques *42*, 446, 448, 450.

EXTENDED EXPERIMENTAL PROCEDURES

Stochastic Model

The simplified two-state model was simulated as described in Experimental Procedures with the reaction scheme and parameters as described in Table S1. The simulations are largely robust to altering basal rates of expression and do not have large effects on circuit activity (Figures S2A and S2B). For stochastic simulations of the more complex, experimentally verified, model (Figure S2C) (Razooky and Weinberger, 2011; Weinberger et al., 2005; Weinberger et al., 2008; Weinberger and Shenk, 2007) BioSpreadSheet was used (http://systems-biology.org/software/simulation/biospreadsheet.html). Parameters and initial conditions are as previously reported in (Razooky and Weinberger, 2011) except that for each parameter set, 1000 simulations were run. At the final time point, a simulation with > 10 Tat molecules is considered 'ON'.

To understand the effect of altering Tat half-life in the model (Figure S2D), 10,000 simulations were run for a specific basal rate of transcription at the native Tat half-life (~8 h). The number of simulations with at least 1 Tat molecule at the end of the simulation was tallied. Next, another 10,000 simulations were run with the Tat half-life reduced by 3.3-fold (to simulate FKBP-mediated decay in absence of Shield-1), and the number of simulations with at least 1 Tat molecule at the end of the simulation was tallied. The difference in the number of ON trajectories for the different Tat half-life was calculated for varying basal rates of transcription.

The simulations of Tat half-life modulation (Figure S2D) suggest that, for specific feedback strengths, altering Tat half-life has the largest affect at a basal rate of transcription of 10^{-5} (Figure S2D). The relationship in Tat half-life to basal rates of transcription has to do with the fact that the FKBP system can only tune protein half-life. Therefore, if the basal rate of transcription is too low, there is no Tat present, and altering the Tat half-life will have no effect (see Figure 4B, clone 1 and Figure S4, clone 7). Alternatively, at very high basal rates of transcription, the majority of the simulations will have a very high ON fraction; therefore, altering Tat half-life will have no effect (see Figure 4D, clone 11 and Figure S4, clone 4). Simulations of the simplified two-state positive-feedback model (Figure S2F) verify that altering Tat half-life has a substantial effect on the percentage of ON trajectories when basal transcription rate falls within a range of low basal rates.

Derivation of Analytic Expression for First Passage Time and Sensitivity Analysis

For the model in Table S1, here we calculate percent of trajectories in the OFF state as a function of time (initial state is $LTR_{ON\ =}$ 1).

Timescale separation:

Since k_{ON}, k_{OFF} < < rest of rates, the exchange between LTR_{ON} and LTR_{OFF} is slow. $LTR_{OFF}(t)$ changes slowly compared to the exchange between LTR_{ON} and $LTR_{ON\text{-}TAT}$ and the production of mRNA and Tat. At each current value of LTR_{OFF} (t), each other compartment is in balance (the in and out flows nearly cancel).

From the balance condition of LTR_{ON_TAT}, we get:

$$LTR_{ON-Tat} = \frac{k_{bind} Tat}{k_{unbind}} LTR_{ON} \tag{1}$$

From the balance of mRNA and protein of *Tat*, we obtain:

$$Tat = \frac{k_p}{\delta_p \delta_m} (k_m LTR_{ON} + k_{transact} LTR_{ON-Tat}) \tag{2}$$

Substituting Equation 1 into 2:

$$Tat = \frac{k_p k_m}{\delta_p \delta_m} LTR_{ON} \left(1 + \frac{k_{transact}}{k_m} \frac{k_{bind}}{k_{unbind}} Tat \right) \tag{3}$$

Assuming strong inequalities valid in the parameter range indicated in Table S1

$$k_{transact} \gg k_m, \ k_{bind} Tat \gg k_{unbind} \tag{4}$$

(2nd inequality can be written as $LTR_{ON-Tat} \gg LTR_{ON}$, Equation 1), we observe that the 2nd term in the parentheses in Equation 3 is much larger than 1. Hence, we can neglect unit in the parentheses in Equation 3, which yields:

$$LTR_{ON} = \frac{\delta_p \delta_m k_{unbind}}{k_p k_{transact} k_{bind}} \tag{5}$$

Note that LTR_{ON} is much smaller than 1, constant in time, and does not depend on k_{ON} and k_{OFF}.

Dynamic equation for LTR_{OFF}, according to the processes in Table S1, has a form:

$$\frac{d}{dt} LTR_{OFF} = - k_{ON} LTR_{OFF} + k_{OFF} LTR_{ON} \tag{6}$$

Assuming that initially population is 100% activated, $LTR_{OFF}(0) = 0$, Equation 6 has the solution

$$LTR_{OFF}(t) = \frac{k_{OFF}}{k_{ON}} LTR_{ON}\left(1 - e^{-k_{ON}t}\right), \tag{7}$$

which approaches a steady state after a long time, $t \sim 1/k_{ON}$. Substituting LTR_{ON} from Equation 5 into 7, we get

$$LTR_{OFF}(t) = \frac{k_{OFF}\delta_p\delta_m k_{unbind}}{k_{ON}k_p k_{transact}k_{bind}}\left(1 - e^{-k_{ON}t}\right) \tag{8}$$

Equation 7 yields the fraction of OFF population as a function of time. The fraction of ON is given mostly by $LTR_{ON\text{-}Tat}(t)$:

$$LTR_{ON-Tat}(t) = 1 - LTR_{ON} - LTR_{OFF}(t) \approx 1 - LTR_{OFF}(t) \tag{9}$$

$$(LTR_{ON} \ll 1, \text{ Eq. } 5).$$

The average level of $Tat(t)$ is determined by Equation 2, where $LTR_{ON-Tat}(t)$ is given by Equations 8 and 9. It decreases in time proportionally to the ON fraction (Equation 9). We note that if the ratio in Equation 8 is larger than 1, which is possible when k_{on} is very small then, at some time point, the whole population goes latent, $LTR_{OFF}(t) = 1$. Otherwise, this ratio represents the eventual OFF fraction:

$$LTR_{OFF}(t \gg 1/k_{ON}) = \frac{k_{OFF}\delta_p\delta_m k_{unbind}}{k_{ON}k_p k_{transact}k_{bind}}. \tag{10}$$

In the opposite initial state (I.e., when initial population is 0% OFF, as given by $LTR_{OFF}(0) = 1$), Equation 6 has the solution:

$$LTR_{OFF}(t) = \frac{k_{OFF}}{k_{ON}} LTR_{ON} + \left(1 - \frac{k_{OFF}}{k_{ON}} LTR_{ON}\right) e^{-k_{ON}t}, \tag{11}$$

which approaches the same steady states (and on the same timescale) as for the previous initial condition (Equation 7), but from the other direction. From Equation 9 we have:

$$LTR_{ON-Tat}(t) = \left(1 - \frac{k_{OFF}}{k_{ON}} LTR_{ON}\right)\left(1 - e^{-k_{ON}t}\right) \tag{12}$$

While $LTR_{OFF}(t)$ in Equation 7 at $t \ll 1/k_{ON}$ is not sensitive to k_{ON} (because k_{ON} cancels out with the Taylor expansion of exponential), the RHS of Equation 12 does depend on k_{ON}.

Ordinary Differential Equation Model

Previous work has established that HIV Tat dynamics and levels, in the transactivated state, can also be described by an ordinary differential equation model (Razooky and Weinberger, 2011; Weinberger and Shenk, 2007):

$$\frac{d}{dt}(Tat) = B_t + \frac{a * Tat}{Km + Tat} - \delta * Tat \tag{13}$$

where B_t is the basal rate of transcription and translation of Tat under assumption of quasi steady-state mRNA production, a is the feedback strength, Km is a Michaelis-Menten constant, and δ is the per capita decay rate of Tat. Since Tat-FKBP half-life, and hence per capita death rate, can be tuned 3.3-fold in the presence versus absence of Shield-1 (Figure 4, main text), the fold change in Tat steady-state was calculated within that dynamic range (Figure S2F). As expected, the system is most sensitive to Tat half-life changes when feedback strength, a, is high and the basal rate of expression, B_t, is low (Figure S2F). The sensitivity to Tat half-life changes also changes in response to Km, as Km will also affect feedback strength (Figures S2G–S2I).

Molecular Cloning Procedures

HIV-d2GFP was designed by replacing GFP in HIV-R7/E$^-$/GFP (Jordan et al., 2003) with d2GFP (Dar et al., 2012). HIV-d2GFP is thus full-length containing d2GFP in place of the Nef gene and a frameshift mutation in the env gene. The HIV-1 LTR promoter driving a DNA fusion of Tat-Dendra (LTD) was generated using fusion PCR with Tat from the LGIT plasmid (Weinberger et al., 2005) and pDendra2-N from Evrogen. The primers were: (1) 5′ Tat-linker-Dendra primer: TCC CGG GGT GTT ACT TCC TCC ACT TCC TCC CTT GTC ATC GTG GTC CTT GTA, (2) 3′ Tat primer: GGG CCC GGA TCC ATG GAG CCA GTA GAT CCT AGA CTA, (3) 5′ Dendra-linker-Tat: GAC GAT GAC AAG GGA GGA AGT GGA GGA AGT AAC ACC CCG GGA ATT AAC CTG, (4) 3′ Dendra primer: GGG CCC CTC GAG TTA CCA CAC CTG GCT GGG CAG GGG GCT. Primers 1 and 3 were added to the PCR reaction at a 50-fold lower concentration than 2 and 4. The GFP-IRES-Tat from LGIT was restriction digested with BamHI and XhoI, and the Tat-Dendra (TD) PCR product was ligated into the backbone of LGIT to generate LTD. The LTD plasmid was used to create the LTDF plasmid. To generate the LTDF

plasmid, the FKBP #24 domain (Chu et al., 2008) from pBMN-HA-YFP-FKBP(E31G-R71G-K105E)-IRES-HcRed-Tandem was amplified using the following primers: (5) FKBP forward: GGA GTG CAG GTG GAA ACC ATC, and (6) FKBP reverse: TCA TTC CAG TTC TAG AAG CTC. The LTD backbone was then amplified using the following primers: (7) Tat-Dendra forward: TTC GAT GTG GAG CTT CTA GAA CTG GAA TGA CTC GAG ACC TGG AAA AAC ATG, and (8) Tat-Dendra reverse: TCC TGG GGA GAT GGT TTC CAC CTG CAC TCC CCA CAC CTG GCT GGG CAG GGG. The two PCR products were then incubated together in an isothermal assembly cocktail as described (Gibson et al., 2009) to generate the LTDF lentiviral vector. pNL4-3 TDF (Tunable-Tat virus) was generated by amplifying TDF from LTDF with the following primers: (9) 5′ Tat-Dendra-FKBP: GGA CCG CGG ATG GAG CCA GTA GAT CCT AGA and (10) 3′ Tat-Dendra-FKBP: GCG TCT AGA TCA TTC CAG TTC GAG AAG CTC CAC ATC GAA GAC GAG AGT GGC ATG TGG. Primer 10 encoded a silent mutation where the third base pair of L105 in FKBP #24 was mutated from A to C to remove an XbaI site. The PCR product was cut with SacII and XbaI. The backbone of a double digest with SacII and XbaI was isolated from the pNL 4-3 ΔTat virus as described (Huang et al., 1994). The backbone and PCR product were then ligated to form pNL4-3 TDF. pNL4-3 TD (Control Virus in text) was generated in the same way as Tunable-Tat Virus but by amplifying TD from LTD with the following primers: (1) 5′ Tat-Dendra: GGA CCG CGG ATG GAG CCA GTA GAT CCT AGA and (2) 3′ Tat-Dendra: GCG TCT AGA TTA CCA CAC CTG GCT GGG CAG GGG GC. The delta-Tat virus was created by restriction digest of the pNL4-3 ΔTat with SacII and XbaI and flipping mCherry into the backbone. To create the LTR-mCherry-IRES-Tat-FKBP construct, we first synthesized d2GFP-IRES-Tat-FKBP, then swapped that into in the LTR-d2GFP-IRES-Tat construct using BamHI and XhoI restriction sites. The sequence of Tat from recombinant clone pNL4-3, GenBank: AAA44985.1, M19921, was used. To clone the LTR-mCherry-IRES-Tat-FKBP construct d2GFP was swapped with mCherry using BamHI and EcoRI restriction sites. To clone the Tet-Tat-Dendra and Tet-Tat-Dendra-FKBP plasmids, Tat-Dendra or Tet-Tat-Dendra was swapped with YFP-Pif from the pHR-TREp-YFP-Pif plasmid (a gift from Wendell Lim's Laboratory, UCSF) using BamHI and NotI restriction sites.

Primary Cell Culture and Staining to Quantify Cellular Activation State

RPMI 1640 (supplemented with L-glutamine, 10% fetal bovine serum, and 1% penicillin-streptomycin) with 20 U/ml r-IL2 (Peprotech, 200-02) was always used to culture primary cells.

Dulbecco's phosphate-buffered saline DPBS (without Calcium and Magnesium) was used for washing and staining. For staining, cells were first washed in fresh media and required volume was removed as unstained control. Cells were then washed once in cold staining buffer (DPBS with 2% FBS) and resuspended in 100ul of staining buffer containing antibody at appropriate dilution (CD25-PE or CD69-APC; BD-PharMingen). Typical antibody was diluted 1 μl in 100ul staining buffer for staining. Cells were left in dark at 4C for 1 hr following which cells were washed with staining solution, DPBS, and then fixed in 1% paraformaldehyde in DPBS.

FACS Sorting Productively Infected Primary Cells

Primary CD4+ T cells were isolated from donor blood and cultured as described. 3 days before infection, cells were activated with αCD3/CD28 beads (Dynabeads) as per manufacturer instructions. Before infection beads were removed. Cells were mixed with appropriate amount of virus (to get ~10% infection) in 100 μl media and spinoculated at 32°C for 2 hr. 4 days post infection, cells were run through strainer capped tubes to break up clumps and taken for FACS. Productively infected cells were isolated by gating for high GFP expression and sorted into media with 20% serum. Post sort, cells were resuspended in standard RPMI media and cultured as before. Cells were removed for antibody staining and fixation on day 9 and 13.

Live/Dead Staining of Cells

Manufacture protocols (Molecular Probes (L-34959)) were followed for live/dead staining of cells. Briefly, cells were washed once with DPBS and resuspended in staining solution (1ml DPBS with 1 μl of yellow stain resuspended in DMSO). Cells were left in dark at 4°C for 1 hr following which cells were washed once with DPBS and fixed in 1% paraformaldehyde in DPBS.

Time-Lapse Single-Cell Imaging and Analysis

Microscopy experiments were performed on a Zeiss Axio Vert inverted fluorescence microscope equipped with a Yokagawa spinning disc, 405-, 488-, and 561-nm laser excitation light sources, CoolSNAP HQ^2 14-bit camera from Photometrics, computer controlled motorized stage, and environmental enclosure, maintaining a temperature of 37°C and a humidified atmosphere with 5% CO_2. Photoconversion was performed by exposing cells to: (*i*) 488 nm (10% laser power, 500 ms exposure time), (*ii*) 561 nm (50% laser power, 500 ms exposure time), (*iii*) 405 nm (100% laser power, 60 s exposure time), (*iv*) 488 nm (10% laser power, 500 ms exposure time), and last of all (*v*) 561 nm light (50% laser power, 500 ms exposure time). Time-lapse experiments immediately followed the photoconversion, and images were captured every 10 min, with a 40x oil, 1.3NA objective, 1 s exposure time, and 50% power on a 561-nm solid-state laser. At least 50 cells were collected for each experiment and analyzed using in-house MATLAB® code as described (Weinberger et al., 2008). Exponential fits for the Tat half-lives were performed on the first 6 hr of microscopy data collected.

SUPPLEMENTAL REFERENCES

Chu, B.W., Banaszynski, L.A., Chen, L.C., and Wandless, T.J. (2008). Recent progress with FKBP-derived destabilizing domains. Bioorg. Med. Chem. Lett. *18*, 5941–5944.

Clotet, B., Bellos, N., Molina, J.M., Cooper, D., Goffard, J.C., Lazzarin, A., Wöhrmann, A., Katlama, C., Wilkin, T., Haubrich, R., et al.; POWER 1 and 2 study groups (2007). Efficacy and safety of darunavir-ritonavir at week 48 in treatment-experienced patients with HIV-1 infection in POWER 1 and 2: a pooled subgroup analysis of data from two randomised trials. Lancet *369*, 1169–1178.

Gibson, D.G., Young, L., Chuang, R.Y., Venter, J.C., Hutchison, C.A., 3rd, and Smith, H.O. (2009). Enzymatic assembly of DNA molecules up to several hundred kilobases. Nat. Methods *6*, 343–345.

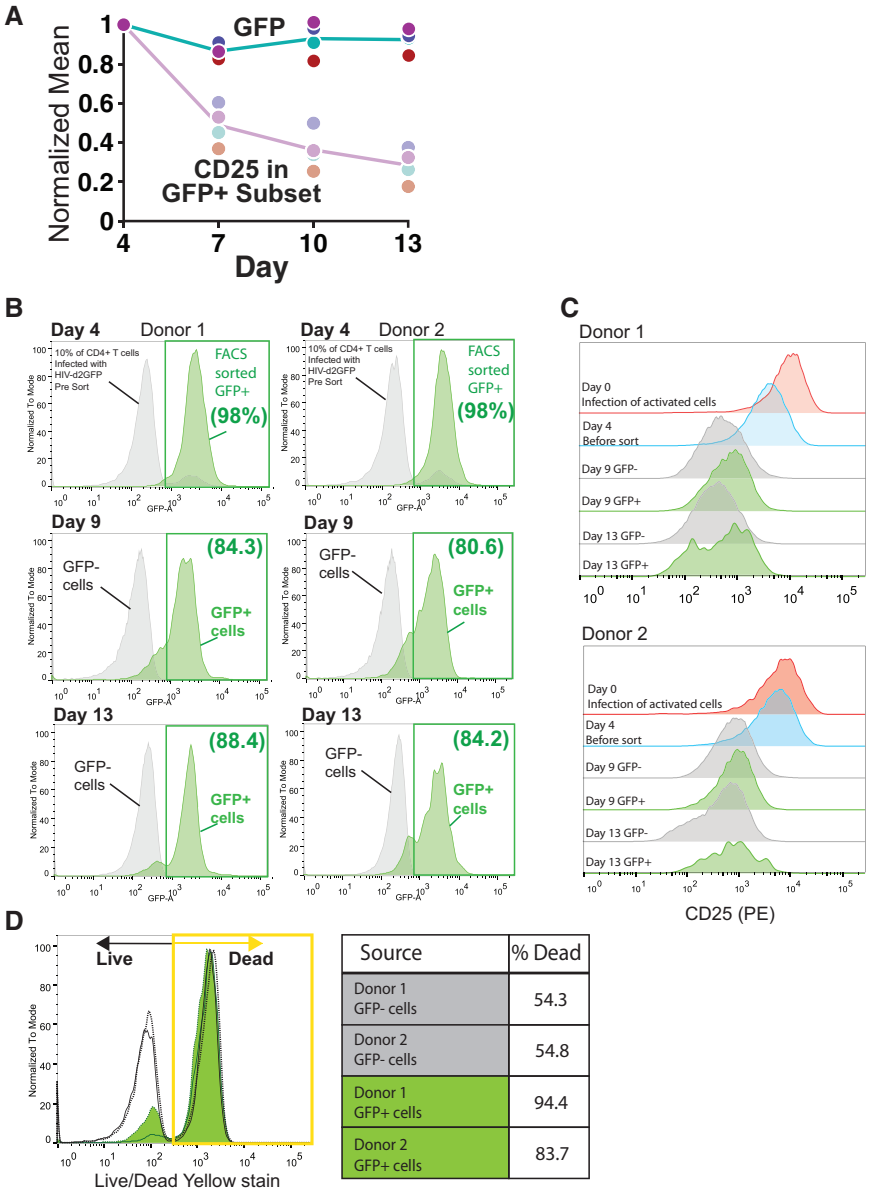

Figure S1. Productively Infected Donor-Derived Primary CD4⁺ T Cells Maintain HIV Expression despite Cellular Relaxation, Related to Figure 2

(A) GFP and CD25 expression of only GFP⁺ cells (normalized to day 4) from experiment shown in Figure 2A. Each dot indicates the time point from an independent infection and represents the geometric mean of the distribution. Solid line connects the mean of the replicates.

(B) Results from FACS sorting of productively infected cells as shown in Figure 2I. Flow cytometry histograms of GFP expression in productively infected primary cells. Shown are the results from two donors for 4 days post infection (day of FACS-based isolation) and days 9 and 13 post infection. Day 4: Grey histogram shows the infected population prior to FACS-based separation. Viral titer used was calibrated to achieve 10% infection (gray cells falling in GFP+ gate marked by green box). Histogram in green shows the GFP expression in the productively infected cells (post sort) isolated using FACS-based sorting. Day 9 and 13: green and gray histograms shows the GFP expression of the isolated GFP+ and GFP- cells. Green box marks the gate for positive GFP expression. Numbers in brackets indicate the proportion of cells that fall within this gate and are clearly separated from the GFP- cells.

(C) Flow cytometry histograms of cellular activation levels measured by CD25-PE staining for both donors. For each donor, the staggered plots display the distribution of the indicated population at the specified day. Activation levels are highest on day of infection (day 0) and decrease rapidly thereafter. The decrease is seen in both GFP- and GFP+ cells.

(D) Flow cytometry histograms of yellow (Live/dead) stain expression after staining of isolated cells at 13 days post infection. Yellow-boxed region indicates the gate for dead fraction. Results from GFP- (unfilled) and GFP+ (green) populations of the two donors (solid and dashed curves are for donor 1 and 2 respectively) are shown. Legend on the right indicates the fraction dead for each population.

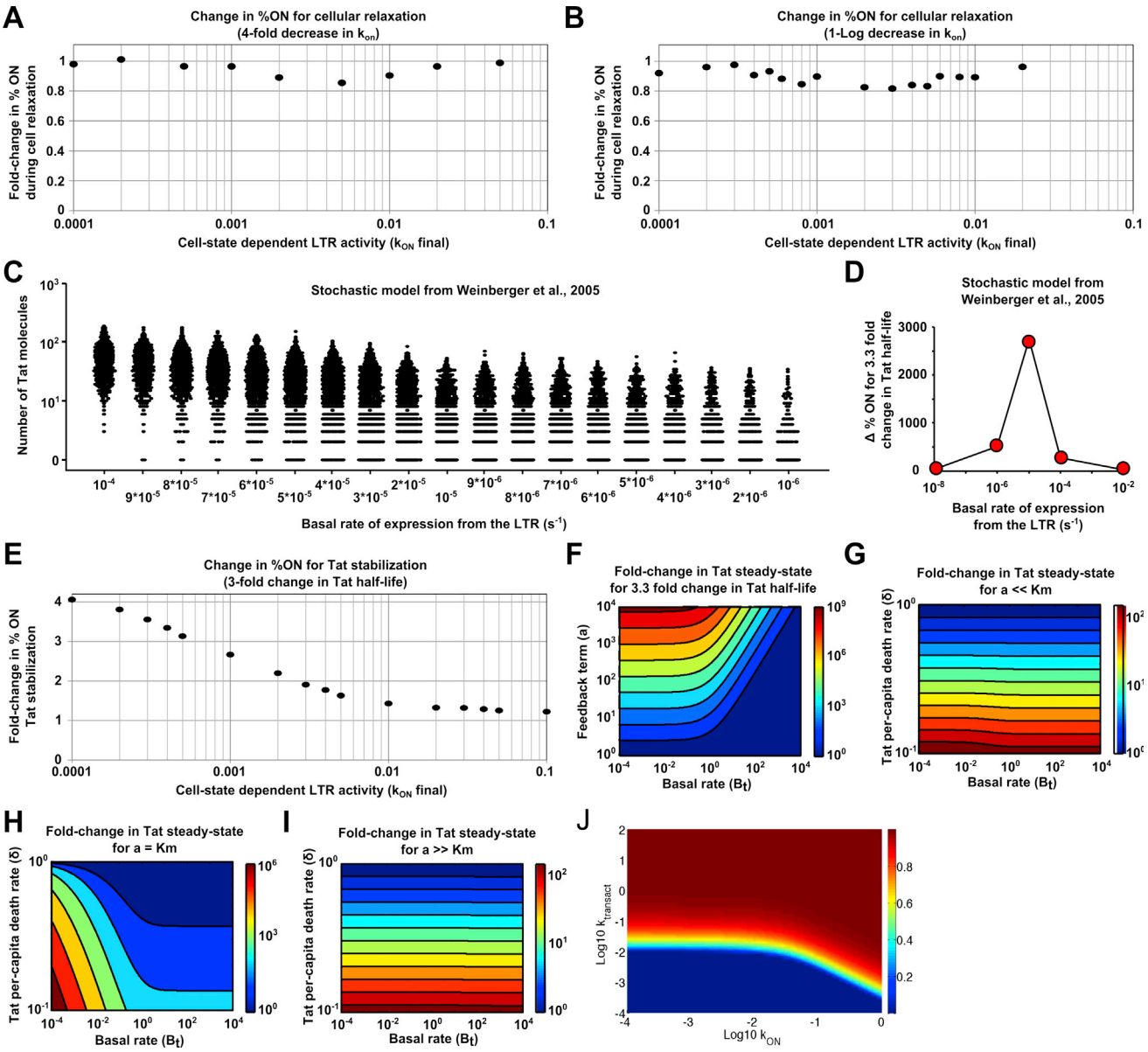

Figure S2. Computational Modeling Indicates Robustness to k_{on} but that Tuning Tat t1/2 Is Sufficient to Reactivate Latent HIV, Related to Figure 3

(A and B) Stochastic simulations of the two-state feedback model (Table S1) showing fold-change in 'ON' for 4-fold or 1-Log changes in k_{on}. Each point represents 1000 runs.

(C and D) Stochastic simulations of a more complex stochastic model of Tat positive feedback (Weinberger et al., 2005) showing Tat molecular number for changing basal rate LTR expression over two orders of magnitude (1000 simulations per parameter set). (D) Fold change in the %ON trajectories (i.e., having > 1 Tat molecule) for a 3.3-fold change in Tat $t_{1/2}$ across varying basal rates of transcription (model and parameters as previously described (Weinberger et al., 2005)).

(E) Change in %ON trajectories for two-state feedback model (Table S1) after 3-fold change in Tat half-life.

(F) Isocline plot of Tat steady state (from ODE model, *Supp. Expt. Procedures*) for a 3.3-fold change in Tat $t_{1/2}$ across different values of Tat feedback strength and basal rate of transcription.

(G–I) Isocline plots of Tat steady state (from ODE model) for changing Tat $t_{1/2}$ under weak ($a << Km$), intermediate ($a = Km$) and strong ($a >> Km$) Tat feedback, respectively.

(J) Phase-plane analysis (sensitivity analysis) of fraction ON as a function of k_{on} and $k_{transact}$ at t = 40h (see analytical derivation Equation [10]). $k_{transact} > k_{on}$ is the physiological parameter regime (Dar et al., 2012; Molle et al., 2007).

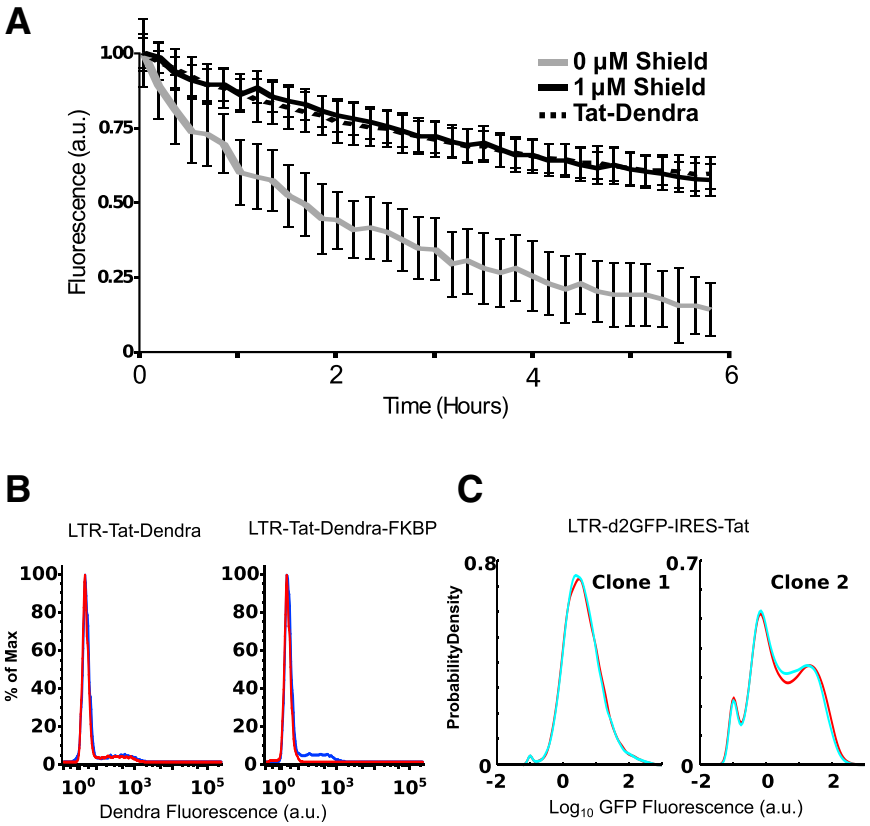

Figure S3. Shield-1 Modulates Tat Half-Life and Does Not Have Measurable Pleiotropic Effects on HIV Positive Feedback, Related to Figure 4

(A) Single-cell pulse-chase analysis of Tat half-life in presence and absence of Shield-1 by time-lapse microscopy. Tat-Dendra half-life determined by assaying the decay in red fluorescence intensity after a rapid pulse of green-to-red photoconversion. Shield-1 increases Tat half-life from ~2.3 hr to ~8 hr in single cells. Error bars indicate SD.

(B) An infected Jurkat LTR-Tat-Dendra population was cultured in the presence (blue) or absence (red) of 1 μM Shield-1. The level of fluorescence in the LTR-Tat-Dendra population does not change upon Shield-1 addition. Incubating an infected Jurkat LTR-Tat-Dendra-FKBP population in the presence (blue) or absence (red) of 1 μM Shield-1 leads to large changes in fluorescence.

(C) Two isoclonal LTR-d2GFP-IRES-Tat populations—*without a FKBP domain*—were incubated in the presence (cyan) or absence (red) of 1 μM Shield-1. Shield-1 did not change expression from the HIV-1 LTR in either population.

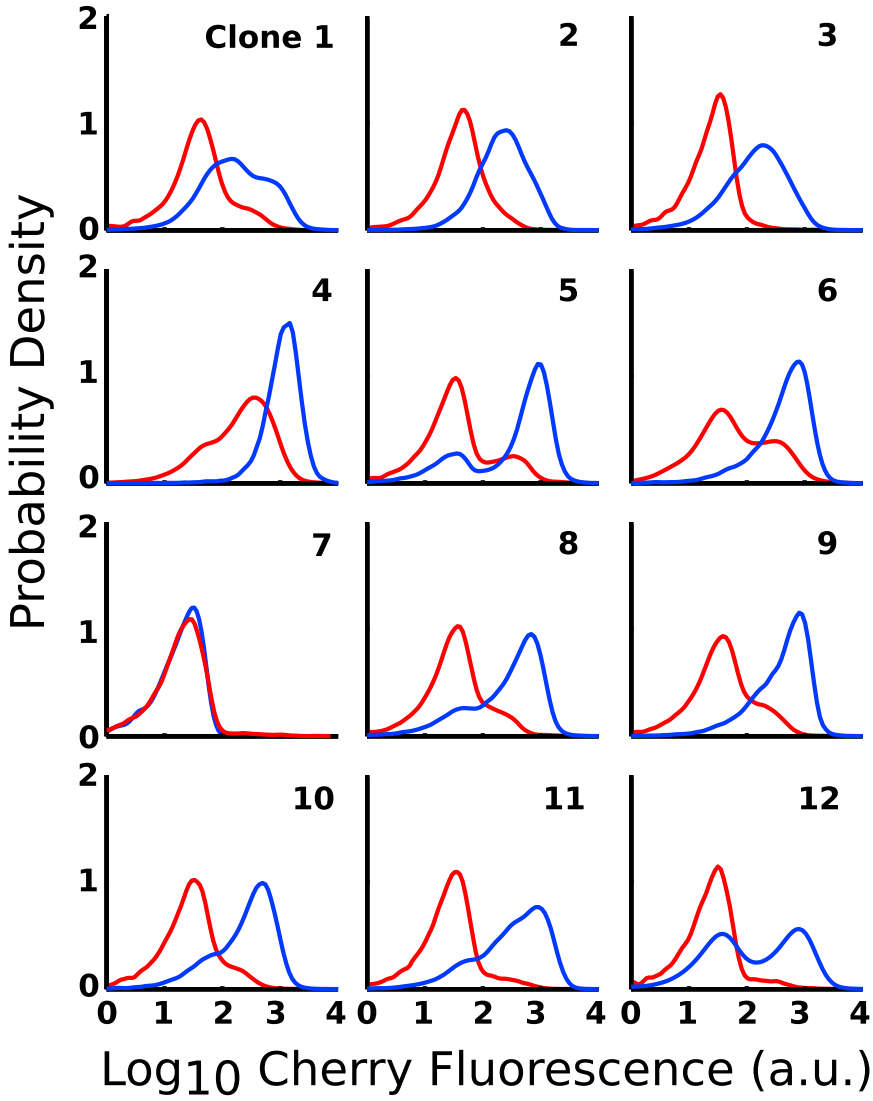

Figure S4. A Decoupled LTR-mCherry-IRES-TatFKBP Circuit Shows that Tuning Tat Half-Life Is Sufficient to Reactivate Latent Clones, Related to Figure 4

Probability distributions of mCherry fluorescence for 12 LTR-Cherry-IRES-Tat-FKBP isoclonal populations with (blue histograms) or without (red histograms) Shield-1. Probability density plots were created using the default ksdensity function in Matlab.

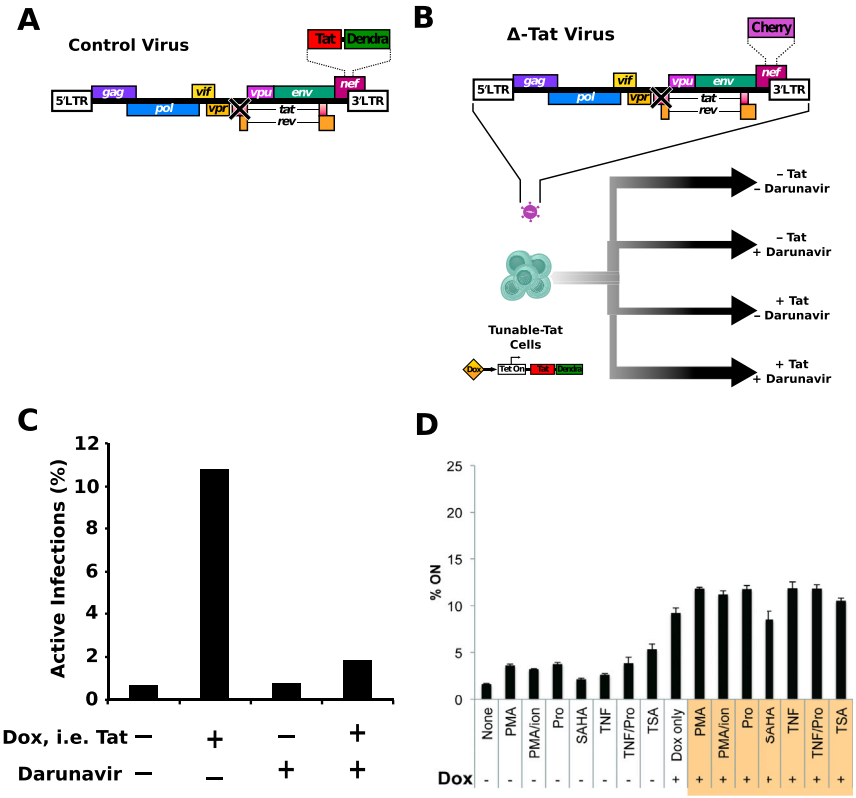

Figure S5. Tat Controls the Percentage of Infections that Are Active or Latent in Replication-Competent, Full-Length HIV, Related to Figure 5

(A) Control HIV was developed as a control virus by placing Tat-Dendra in the *nef* reading frame. Multiple premature stop codons were placed in the native Tat reading frame to prevent expression of Tat from the native locus.

(B) To check for replication competency of the delta-Tat virus (B), Tunable-Tat cells were infected with delta-Tat virus in the presence or absence of doxycycline and Darunavir (a protease inhibitor (Clotet et al., 2007)).

(C) Five days post infection, in the absence of both, only 0.8% of cells were actively infected, while in the presence of doxycycline 10.8% of cells were actively infected. In the presence of Darunavir the virus did not replicate in the absence, 1% actively infected, or presence, 2.5% actively infected, of doxycycline.

(D) Jurkat 'Inducible-Tat Cells' (Dox-inducible Tat-dendra) were infected with full-length ΔTat-Cherry virus in triplicate. 3 days post infection, cells were treated with indicated compounds (or none). Shown are % ON cells by flow cytometry. Colored area indicates combination of Dox with indicated cell state modifier. Data shown here is from experiment independent of that shown in Figure 5E. Error bars indicate SD.

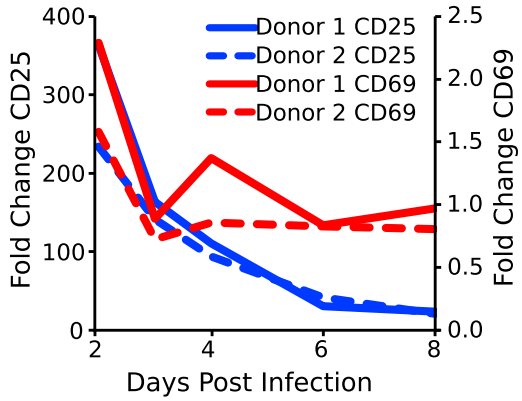

Figure S6. Activation and Relaxation Dynamics of Primary Cells, Related to Figure 6

Relaxation kinetics from two donors (Donor 1, solid lines and Donor 2, dashed lines) and the fold change in the levels of CD25 (green) and CD69 (purple) are shown. Green lines correspond to CD25 y axis on the left, and the purple lines correspond to the CD69 y axis on the right. Time points were taken at 2, 3, 4, 6, and 8 days. At day 2 post infection, CD3/CD28 beads, IL-2, and virus were removed from the culture to allow the activated cells to relax back to the resting state.